Room-temperature disorder-driven nonlinear transport in topological materials

Rhonald Burgos Atencia,[1,2,3] Shanshan Liu,[4] Kian Ping Loh,[4] and Dimitrie Culcer[1,2]
[1]*School of Physics, The University of New South Wales, Sydney 2052, Australia*
[2]*ARC Centre of Excellence in Low-Energy Electronics Technologies, UNSW Node, The University of New South Wales, Sydney 2052, Australia*
[3]*Dipartimento di Fisica "E. R. Caianiello", Università di Salerno, IT-84084 Fisciano (SA), Italy*
[4]*Department of Chemistry, National University of Singapore, Singapore 117543, Singapore*

(Received 16 June 2025; revised 10 October 2025; accepted 4 May 2026; published 26 May 2026)

Recent experiments have reported nonlinear signals in topological materials up to room temperature. Here we show that this response stems from extrinsic spin-orbit contributions to both impurity and phonon scattering. While skew scattering dominates at low temperatures, the side jump contribution $\propto\tau/\tau_\beta$, where τ, τ_β are the momentum and skew scattering times, respectively. Consequently side jump exhibits a weak temperature dependence and remains sizable at room temperature. Our results provide a roadmap for engineering nonlinear transport at ambient conditions.

DOI: 10.1103/58gz-d7zc

I. INTRODUCTION

Nonlinear electrical transport has emerged as a powerful probe of symmetry [1–5], band geometry [6,7], and scattering processes in quantum materials [8]. A striking manifestation is the nonlinear Hall effect (NLHE), which occurs even in time-reversal symmetric systems [9,10]. Remarkably, recent experiments have reported a robust NLHE persisting up to room temperature in spin-orbit-coupled materials, notably in bismuth [11], $BaMnSb_2$ [12], and Sb-doped topological insulators such as $MnBi_4Te_7$ [13], among others [14–16]. This offers significant potential for applications in, e.g., terahertz technologies [17–21], photodetection [22,23], nonvolatile memory [24] and rectification [25–28].

Disorder is naturally present in realistic samples [10,29–32], and disorder-mediated contributions play a significant role even in $\mathcal{PT}$-symmetric systems [8,33], where $\mathcal{P}$ stands for inversion and $\mathcal{T}$ for time reversal. The Berry curvature dipole (BCD), often responsible for intrinsic responses [34–36], is suppressed when additional crystal symmetries are present, as occurs, for instance, in topological insulator surface states with threefold rotational symmetry [9]. In such scenarios, extrinsic mechanisms—side-jump and skew-scattering—may dominate the nonlinear response [10,37,38]. This was experimentally observed recently, with NLHE signals persisting up to room temperature [39]. The understanding of disorder in nonlinear responses remains limited, while the role of phonons, to our knowledge, has never been considered explicitly, precluding a systematic understanding of room-temperature effects. These observations highlight the need for a new theoretical perspective on disorder effects in nonlinear transport.

Motivated by this, our work focuses on nonlinear responses that arise from extrinsic scattering processes, particularly in regimes where intrinsic effects are suppressed by symmetry [39]. We develop a rigorous general framework based on the quantum Liouville equation that consistently incorporates disorder and phonon scattering as well as extrinsic spin-orbit coupling in the scattering potentials. Our approach captures skew scattering and side jump stemming from both disorder and phonons, the temperature dependence of the nonlinear response, and the interplay between disorder and lattice effects. Our central result is the transversal nonlinear susceptibility

$$\chi_{xyy} = C_1\frac{\tau^3}{\tau_\beta} + C_2\frac{\tau}{\tau_\beta}, \tag{1}$$

where C_1 and C_2 are functions of the Fermi energy, τ is the momentum relaxation time, and τ_β is a characteristic skew-scattering time associated with extrinsic spin-orbit scattering. Since the linear longitudinal conductivity σ_{xx} is usually given by the Drude formula $\propto\tau$, the interplay of phonon and disorder scattering results in NLHE signals scaling as σ_{xx} and σ_{xx}^3. The survival of the nonlinear signal up to room temperature [39] is explained as follows. When the temperature increases, both scalar scattering and spin-orbit scattering are affected, so that τ and τ_β decrease substantially, and the skew scattering contribution $\propto\tau^3/\tau_\beta$ becomes vanishingly small. However, the side-jump contribution $\propto\tau/\tau_\beta$ such that the temperature dependences of τ and τ_β partially compensate each other. This results in a weak temperature dependence of the side jump, so that the side-jump signal remains strong at room temperature.

The results provide a key step toward understanding and controlling nonlinear charge dynamics for electronics and sensing. First, the side jump is expected to survive to high temperatures quite generally, making it a useful mechanism

Published by the American Physical Society under the terms of the Creative Commons Attribution 4.0 International license. Further distribution of this work must maintain attribution to the author(s) and the published article's title, journal citation, and DOI.

for room-temperature applications. Second, given the strong mobility dependence of the skew-scattering contribution, an improvement in the mobility by an order of magnitude could enhance the low-temperature nonlinear signal by 10^3. Finally, the strategy presented here can be extended to third-order responses [40–48].

II. GENERAL FORMALISM AND MODEL HAMILTONIAN

Our approach is based on the solution of the quantum Liouville equation for the density matrix ρ, namely,

$$\partial_t \rho + (i/\hbar)[H, \rho] = 0, \tag{2}$$

where H is the Hamiltonian of the systems. In general, the Hamiltonian is written as

$$H = H_0 + H_E + U(\boldsymbol{r}), \tag{3}$$

where H_0 is the unperturbed band Hamiltonian, $H_E(\boldsymbol{r}) = e\boldsymbol{E}\cdot\boldsymbol{r}$ is the external driving term, and $U(\boldsymbol{r})$ is the disorder potential. Importantly, in topological materials with strong spin-orbit interactions the scattering potential itself contains an extrinsic spin-orbit term. Such a term is known in topological insulators, where it affects STM quasiparticle interference [49] and weak localization [50]. In our case such an extrinsic spin-orbit term is present in the phonon as well as in the impurity scattering potentials. We will focus on its effect on impurity scattering.

The solution of the evolution equation for ρ follows straightforward steps described in Ref. [51–53] (see also Appendix A). Expressing the kinetic equation in the crystal momentum representation we find the equation

$$\frac{\partial f}{\partial t} + \frac{i}{\hbar}[H_0, f] + J_0(f) = \frac{e\boldsymbol{E}}{\hbar}\cdot\frac{Df}{D\boldsymbol{k}} - J_E(f), \tag{4}$$

with $f_{\boldsymbol{k}}$ the disorder-averaged part of the density matrix ρ expressed in the crystal momentum representation. Also, the covariant derivative is defined as

$$\frac{Df}{D\boldsymbol{k}} = \frac{df}{d\boldsymbol{k}} + i[f, \boldsymbol{\mathcal{R}}], \tag{5}$$

where the Berry connection vector reads

$$\boldsymbol{\mathcal{R}}^{mm'} = i\langle u_{\boldsymbol{k}}^m | \nabla_{\boldsymbol{k}} u_{\boldsymbol{k}}^{m'}\rangle \tag{6}$$

and $|u_{\boldsymbol{k}}^{m'}\rangle$ are periodic part of the Bloch eigen states of the unperturbed Hamiltonian. The collision integrals $J_0(f)$ and $J_E(f)$ are defined as

$$\begin{aligned} J_0(f) &= \frac{1}{2\pi\hbar}\int_{-\infty}^{\infty} d\epsilon \langle [U, G^R(\epsilon)[U, f]G^A(\epsilon)]\rangle \\ J_E(f) &= \frac{1}{2\pi\hbar}\int_{-\infty}^{\infty} d\epsilon \langle [U, G^R(\epsilon)[H_E, g_0]G^A(\epsilon)]\rangle \end{aligned} \tag{7}$$

with $G^{R/A}(\epsilon)$ retarded and advanced free Green's functions [52] in the frequency domain ϵ and $\langle\cdots\rangle$ refers to the impurity average. Also,

$$g_0 = \frac{1}{2\pi i}\int_{-\infty}^{\infty} d\epsilon G^R(\epsilon)[U, f]G^A(\epsilon). \tag{8}$$

To account for the temperature dependence of transport properties, it is essential to include electron-phonon interactions, which yield an additional relaxation mechanism. The corresponding collision integral is given by [54–60]:

$$\begin{aligned} [J_{\rm ep}(f)]_{\boldsymbol{k}}^{++} = &-\frac{2\pi}{\hbar}\sum_{\boldsymbol{q}} |D_{\boldsymbol{q}}|^2 \delta(\hbar\omega_{\boldsymbol{q}} + \varepsilon_{\boldsymbol{k}-\boldsymbol{q}}^+ - \varepsilon_{\boldsymbol{k}}^+) \\ &\times [N_{\boldsymbol{q}} f_{\boldsymbol{k}-\boldsymbol{q}}^+(1 - f_{\boldsymbol{k}}^+) - (1 + N_{\boldsymbol{q}}) f_{\boldsymbol{k}}^+(1 - f_{\boldsymbol{k}-\boldsymbol{q}}^+)] \\ &-\frac{2\pi}{\hbar}\sum_{\boldsymbol{q}} |D_{\boldsymbol{q}}|^2 \delta(\hbar\omega_{\boldsymbol{q}} + \varepsilon_{\boldsymbol{k}}^+ - \varepsilon_{\boldsymbol{k}+\boldsymbol{q}}^+) \\ &\times [(1 + N_{\boldsymbol{q}}) f_{\boldsymbol{k}+\boldsymbol{q}}^+(1 - f_{\boldsymbol{k}}^+) - N_{\boldsymbol{q}} f_{\boldsymbol{k}}^+(1 - f_{\boldsymbol{k}+\boldsymbol{q}}^+)], \end{aligned} \tag{9}$$

where $N_{\boldsymbol{q}}$ denotes the phonon occupation number. The electron-phonon coupling is described by the deformation potential $D_{\boldsymbol{q}}$. In the Appendix F we provide the full derivation of the electron-phonon relaxation time.

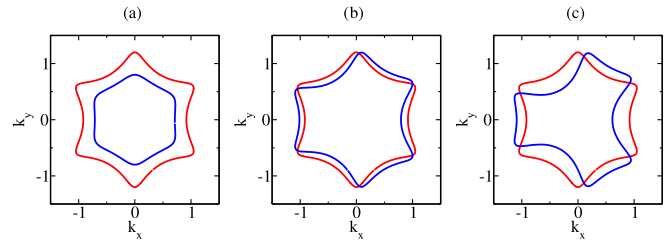


FIG. 1. Isoenergy plots. Momentum are measured in units of $k^* = \sqrt{v_F/\lambda}$ and the energies are in units of $\varepsilon^* = v_F k^*$. The Fermi velocity is $v_F = 1.01$ eV Å and we take the warping parameter $\lambda = 250$ Å. (a) We took $\Delta = 0$ with $\varepsilon_F = 1.2\varepsilon^*$ and $\varepsilon_F = 0.8\varepsilon^*$ for red and blue, respectively. (b) We fixed $\varepsilon_F = 1.2\varepsilon^*$ and take $\Delta/\varepsilon^* = 0$ and $\Delta = 0.4\varepsilon^*$ for the red and blue lines, respectively. (c) We fixed $\varepsilon_F = 1.2\varepsilon^*$ and take $\Delta/\varepsilon^* = 0$ and $\Delta/\varepsilon^* = 0.8$ for the red and blue lines, respectively.

A. Model Hamiltonian

The band Hamiltonian for topological insulators with warping can be cast as [61,62]

$$H_0 = \hbar v_F(k_x\sigma_y - k_y\sigma_x) + \frac{\lambda}{2}(k_+^3 + k_-^3)\sigma_z + \Delta\sigma_z, \tag{10}$$

with λ the warping coupling, Δ is half the gap and the definition

$$k_\pm = k_x \pm ik_y = ke^{\pm i\theta}. \tag{11}$$

The warping term can also be written as $H_w = \lambda k^3\cos(3\theta_{\boldsymbol{k}})\sigma_z$ with $\theta_{\boldsymbol{k}} = \arctan(k_y/k_x)$. Written in this form, the warping term reflects the sixfold symmetry of the band Hamiltonian. The dispersion relation is

$$\varepsilon_{\boldsymbol{k}}^{\pm} = \pm\sqrt{(\hbar v_F k)^2 + M_z^2}, \tag{12}$$

where $M_z = \Delta + \lambda k^3\cos(3\theta_{\boldsymbol{k}})$. In order to have a nonlinear response we need to break at least one mirror symmetry. In our systems this is done jointly by the gap and the warping parameter. For $\Delta = 0$ the system has the sixfold symmetry while for $\Delta \neq 0$ the mirror symmetry is broken along k_y. The bigger the gap, the more the deviation from the sixfold rotation. In Fig. 1, we illustrate the disappearance of sixfold symmetry when $\Delta \neq 0$. As the gap increases, the deviation

from sixfold rotational symmetry becomes more pronounced. Furthermore, the absence of an inversion center enhances the potential for nonlinear conductivity.

In terms of the parameter

$$\xi_k = \frac{\Delta + \lambda k^3 \cos(3\theta_{\boldsymbol{k}})}{\varepsilon_{\boldsymbol{k}}} \tag{13}$$

the states can be written as

$$|u_{\boldsymbol{k}}^{\pm}\rangle = \frac{1}{\sqrt{2}} \begin{pmatrix} e^{-i\theta_{\boldsymbol{k}}}\sqrt{1 \pm \xi_k} \\ \pm i\sqrt{1 \mp \xi_k} \end{pmatrix}. \tag{14}$$

We consider here two independent sources of scattering. One is related the scalar scattering potential $U_0(\boldsymbol{r})$ that will define a relaxation time τ. The other mechanism is related the extrinsic spin-obit coupling and can be cast as $U_{\boldsymbol{k},\boldsymbol{k}'} = i\beta\boldsymbol{\sigma} \cdot \boldsymbol{k} \times \boldsymbol{k}'$, defining a relaxation time $1/\tau_\beta = \pi\rho(\epsilon_F)[u_0^2\beta^2 k_F^4]/\hbar$, with $\rho(\epsilon_F)$ the density of states at the Fermi energy, u_0^2 the strength of the scattering potential and β the extrinsic spin-orbit strength. Disorder plays an important role in the dynamics as experiments also show in a renormalization of the nonlinear response [39,63,64]. This experimental fact motivates us to include two sources of scattering, where one will account for restoring $\mathcal{T}$ symmetry and one will account for stabilizing Fermi surface.

III. RESULTS

A. Leading response

We solve the kinetic equation (A5) for the distribution function $f_{\boldsymbol{k}}$ up to second order in the electric field [8]. For convenience in notation, we separate the function $f_{\boldsymbol{k}}$ into a band diagonal and an off-diagonal contribution as

$$f_{\boldsymbol{k}}^{mm'} = n_{\boldsymbol{k}}^{mm'}\delta_{mm'} + S_{\boldsymbol{k}}^{mm'}. \tag{15}$$

The leading distribution to second order in the electric field is diagonal in band index and satisfies the kinetic equation

$$\left[J_0\left(n_{E2}^{(-2)}\right)\right]_{\boldsymbol{k}}^{mm} = (e/\hbar)\boldsymbol{E} \cdot \boldsymbol{\nabla}_{\boldsymbol{k}} n_{E\boldsymbol{k}}^{(-1)mm}. \tag{16}$$

Then we solve for $n_{E2}^{(-2)mm}$ in the relaxation time approximation. In the driving term, the distribution $n_{E\boldsymbol{k}}^{(-1)mm}$ is the leading-order linear Boltzmann distribution, which is straightforward to calculate [52]. Once we calculate the distribution $n_{E2\boldsymbol{k}}^{(-2)mm}$ we can use it to generate a new driving term. In our notation, the superscript in the distribution means its scaling with respect to impurity density. This follows from the collision integral of extrinsic spin-orbit coupling impurities. The kinetic equation to be solved is

$$\left[J_0\left(n_{E2\beta}^{(-2)}\right)\right]_{\boldsymbol{k}}^{mm} = -\left[J_\beta\left(n_{E2}^{(-2)}\right)\right]_{\boldsymbol{k}}^{mm}, \tag{17}$$

where the right-hand side is a driving term and β means that in the collision integral we use the extrinsic spin orbit potential. This will provide the nonlinear distribution $n_{E2\beta}^{(-2)} \propto \tau^3/\tau_\beta$, which will explain the cubic behavior of experimental data with respect to relaxation time (see Appendixes B and C for the full derivation). After a straightforward calculation we find the susceptibility

$$\left[\chi_{xyy}^{(-2)}\right] = \lambda\left(\frac{\tau^3}{\tau_\beta}\right)\left(\frac{e^3}{\hbar}\right)\frac{\rho(\varepsilon_F)\left(1-\xi_F^2\right)\varepsilon_F}{\hbar^2}H(\xi_F), \tag{18}$$

with the density of states $\rho(\varepsilon_F) = \varepsilon_F/2\pi\hbar^2 v_F^2$ and dimensionless

$$H(\xi_F) = (1/64)\left(15\xi_F + 13\xi_F^3 - 75\xi_F^5 + 33\xi_F^7\right) \tag{19}$$

with $\xi_F = \Delta/\varepsilon_F$.

B. Interband coherence effect

The nonlinear response observed in experiments also exhibits a linear dependence on the longitudinal conductivity, which is traced to a linear scaling with the relaxation time. This contribution is highly nontrivial and constitutes one of the central results of our work. Interestingly, this subleading response is entirely driven by interband transitions. At the microscopic level, the overall effect combines side-jump and skew-scattering processes. To account for the observed linear-in-τ behavior, the dominant ingredient is the linear side-jump effect [52,65]. From a semiclassical perspective, it was shown in Refs. [66–68] that the side-jump mechanism can be formulated in terms of a coordinate shift. In the present work, we address the problem within a fully quantum mechanical framework, which rigorously captures the role of the Berry curvature and is in full correspondence with the semiclassical coordinate-shift picture [8]. The procedure starts by calculating the linear side-jump distribution, denoted as $n_{E\boldsymbol{k},sj}^{(0)mm}$, which follows from the electric-field-corrected collision integral in Eq. (7), with $U(\boldsymbol{r})$ representing the full scattering potential. The collision integral acts as a driving term. As we explain in Appendix D, it is convenient to decompose the driving term into two distinct contributions: one associated with the scalar potential and the other with the spin-orbit potential. In this way, the linear side-jump effect naturally separates into two parts,

$$n_{E\boldsymbol{k},sj}^{(0)mm} = n_{E\boldsymbol{k}}^{(0)mm} + n_{E\boldsymbol{k},\beta}^{(0)mm}, \tag{20}$$

where the first and second terms correspond to coordinate shifts induced by scalar and spin-orbit scattering, respectively. The second-order distribution follows from the equation

$$\left[J_0\left(n_{E2,sj}^{(-1)}\right)\right]_{\boldsymbol{k}}^{mm} = (e/\hbar)\boldsymbol{E} \cdot \boldsymbol{\nabla}_{\boldsymbol{k}} n_{E\boldsymbol{k},sj}^{(0)mm} \tag{21}$$

and can be further decomposed into

$$n_{E2\boldsymbol{k},sj}^{(-1)mm} \to n_{E2}^{(-1)mm} + n_{E2,\beta}^{(-1)mm}. \tag{22}$$

The next step is to calculate the off-diagonal distribution

$$S_{E2\boldsymbol{k},\beta}^{(0)mm'} = i\hbar\left(\epsilon_{\boldsymbol{k}}^m - \epsilon_{\boldsymbol{k}}^{m'}\right)^{-1}\left(\left[J_\beta\left(n_{E2}^{(-1)}\right)\right]_{\boldsymbol{k}}^{mm'} + \left[J_0\left(n_{E2,\beta}^{(-1)}\right)\right]_{\boldsymbol{k}}^{mm'}\right), \tag{23}$$

as detailed in Appendix D. The current is then obtained by tracing the off-diagonal velocity,

$$v_a^{mm'} = i\hbar^{-1}\left(\varepsilon_{\boldsymbol{k}}^m - \varepsilon_{\boldsymbol{k}}^{m'}\right)\mathcal{R}_a^{mm'} \tag{24}$$

with the corresponding off-diagonal distribution. We emphasize that interband coherence effects become particularly pronounced at second order, owing to the quantum-mechanical nature of both the off-diagonal distribution and the off-diagonal velocity. Notably, the latter is directly governed by the Berry connection, highlighting once again the central role of geometric properties of the band structure in driving the side-jump effect.

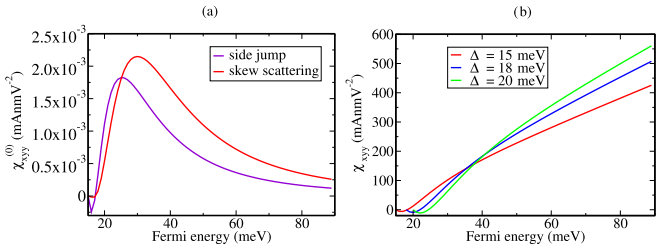


FIG. 2. (a) Nonlinear subleading susceptibility as a function of the Fermi energy. We take $v_F = 1.6 \times 10^5$ m/s, the warping constant $\lambda = 80\,\mathrm{eV}^3$ and $\tau = 1$ ps and $\tau_\beta = 0.5$ ps. We fixed the $\Delta = 15$ meV. (b) Total nonlinear susceptibility as a function of the Fermi energy. We take $v_F = 1.6 \times 10^5$ m/s, the warping constant $\lambda = 80\,\mathrm{eV}^3$ and $\tau = 1$ ps and $\tau_\beta = 0.5$ ps.

There exists also a skew-scattering contribution of the same order as the side-jump effect [8,52]. This mechanism involves interband transitions that manifest within the diagonal group velocity. Physically, this effect originates from an electron undergoing successive scattering events, during which it transiently explores different bands before returning to its original one (virtual transitions [67]). Formally, the contribution is obtained by solving the kinetic equation

$$\left[J_0\left(n^{(0)}_{E2,\beta}\right)\right]^{mm}_{\boldsymbol{k}} = -\left[J_0\left(S^{(0)}_{E2,\beta}\right)\right]^{mm}_{\boldsymbol{k}} - \left[J_\beta\left(S^{(0)}_{E2}\right)\right]^{mm}_{\boldsymbol{k}}. \tag{25}$$

Here the renormalized off-diagonal distribution is already known, however, the second driving term requires the β-independent off-diagonal distribution,

$$S^{(0)mm'}_{E2\boldsymbol{k}} = i\hbar\left(\epsilon^m_{\boldsymbol{k}} - \epsilon^{m'}_{\boldsymbol{k}}\right)^{-1}\left(\left[J_0\left(n^{(-1)}_{E2,\beta}\right)\right]^{mm'}_{\boldsymbol{k}}\right). \tag{26}$$

In summary, interband transitions also underlie the skew-scattering mechanism and thus provide a unified explanation for the experimentally observed linear-in-relaxation-time scaling of the nonlinear response (see Appendixes D and E). The full subleading susceptibility, which combines both side jump and skew scattering, is then written as

$$\left[\chi^{(0)}_{xyy}\right] = -\lambda\left(\frac{\tau}{\tau_\beta}\right)\left(\frac{e^3}{\hbar}\right)\frac{\rho(\varepsilon_F)}{\epsilon_F}\left(1-\xi_F^2\right)G(\xi_F) \tag{27}$$

with the dimensionless function

$$G(\xi_F) = \frac{4}{512}\left\{\left(1-\xi_F^2\right)\left[\left(10\xi_F^3 + 54\xi_F^5 - 36\xi_F^7\right)\right] + \left(1-\xi_F^2\right)^{1/2}\left[-88\xi_F^3 + 128\xi_F^5 - 24\xi_F^7\right]\right\}. \tag{28}$$

We plot the separate contributions in Fig. 2(a). The function $G(\xi_F)$ scales with powers of inverse Fermi energy, what explains the rapid decay of the subleading contribution. Side jump and skew scattering cannot be distinguished experimentally: although they depend differently on the Fermi energy they are of the same order of magnitude, as in linear response [52].

In the diffusive regime considered here the term $\chi^{(-2)}_{xyy}$ dominates the susceptibility, which is explicit in the prefactor $\varepsilon_F\tau/\hbar \gg 1$ in Eq. (18). We plot

$$\chi_{xyy} = \chi^{(0)}_{xyy} + \chi^{(-2)}_{xyy} \tag{29}$$

in Fig. 2(b) as a function of the Fermi energy. The increase with Fermi energy is also seen in experiments [39]. Such a behavior is dominated by $\chi^{(-2)}_{xyy}$ precisely by the factor indicating diffusive regime, which scales as $\sim\varepsilon_F^2$. Note that the dominant contribution in $H(\varepsilon_F)$ scales as $\sim 1/\varepsilon_F$. All this will provide the linear increase in the response as a function of the Fermi energy.

C. Scattering by phonons

Phonon scattering becomes relevant as the temperature increases. Solving the electron-phonon collision integral Eq. (9) (see Appendix F) in the relaxation time approximation we find

$$\frac{1}{\tau_{\mathrm{ph}}} \approx \left(\frac{k_B T}{\hbar}\right)\left(\frac{c_R^4 C}{2c_l^4\pi\eta\rho_M c_R^2}\right)\left(\frac{\alpha^2}{\hbar^2}\right)(2k_F), \tag{30}$$

where we have used the deformation potential of Ref. [58]:

$$D_{\boldsymbol{q}} = \alpha\sqrt{\frac{C}{qA}}\left(\frac{\omega^{(0)}_q}{c_l}\right)^2\sqrt{\frac{\hbar}{2\rho_M\omega^{(0)}_q}}\Lambda_l(q), \tag{31}$$

with $\Lambda_l(q) \approx 1$ and A is the area of the unit cell. For Bi_2Te_3 the parameter $\alpha = 35$ eV, $C = 1.2$, $c_l = 2800$ m/s is the longitudinal phonon velocity. $\rho_M = 7861\ \mathrm{kg/m^3}$ is the mass density of the material, and $\omega = c_R q$ where $c_R = 0.86 c_t$ with the transversal phonon velocity $c_t = 1600$ m/s. We recall that $1/\eta = \Delta/v_F^2$ is an effective mass (see Appendix F).

IV. DISCUSSION

In $\mathcal{PT}$-broken systems, the response scales linearly with τ. In these systems, the BCD has attracted considerable attention [69,70] due to its strong sensitivity to band structure [71–74], although it is constrained by crystal symmetries. Even when symmetry allows, side-jump and skew-scattering contributions can compete with the BCD, making experimental identification challenging [10]. In contrast, for $\mathcal{PT}$-symmetric systems the response consists of two distinct terms: one scaling as τ^2 and another as τ^0 [8]. In this case, the BCD is forbidden, and the quantum metric emerges as the intrinsic band-related mechanism [75–78]. Importantly, the τ^0 term denotes independence of the impurity density, resulting from competing relaxation processes that both scale linearly with impurity concentration—a phenomenon already familiar from linear response [52,68].

At finite temperature, disorder dependence changes due to two effects: (i) above the N'eel temperature, thermal fluctuations restore time-reversal symmetry [79], placing the system in a $\mathcal{PT}$-broken regime with modified scaling. Experiments report τ^3 and τ contributions [63,80–82], consistent with phenomenological models of the anomalous Hall effect [83,84]. (ii) Phonon-induced relaxation, included via Matthiessen's rule

$$\tau^{-1} \to \tau^{-1} + \tau_{\mathrm{ph}}^{-1} \tag{32}$$

(and similarly for τ_β^{-1}), introduces an additional effective channel τ_β that renormalizes the nonlinear conductivity.

Applying Matthiessen's rule to Eq. (1), the second-order susceptibility takes the form

$$\chi_{xyy}(T) = (1+AT)[B(1+DT)^{-1} + F(1+DT)^{-3}], \tag{33}$$

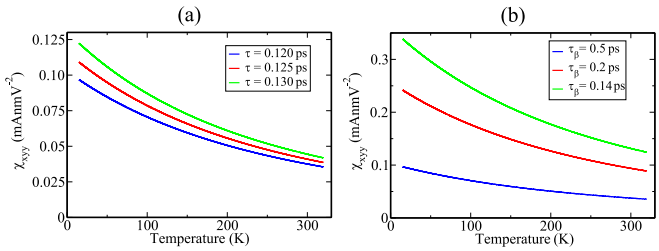


FIG. 3. Total nonlinear susceptibility as a function of the temperature. (a) We take $v_F = 1.6 \times 10^5$ m/s, the warping constant $\lambda = 80\,\mathrm{eV}^3$ and $\Delta = 15$ meV, $\varepsilon_F = 25$ meV, and $\tau_\beta = 0.2$ ps and changed the momentum relaxation time. (b) We fixed $\tau = 0.12$ ps and changed τ_β.

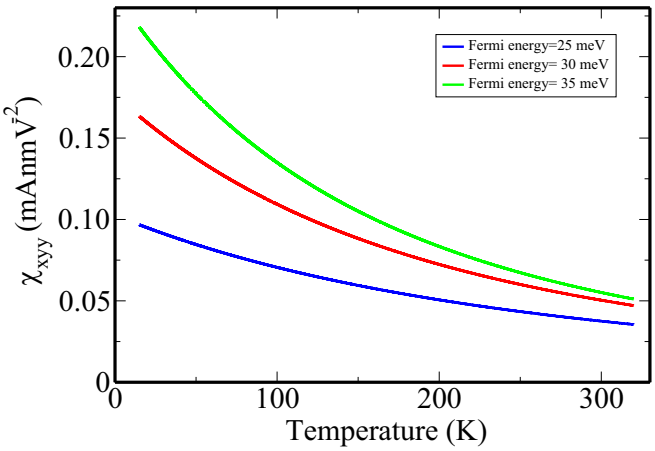


FIG. 4. Total nonlinear susceptibility as a function of the temperature. We take $v_F = 1.6 \times 10^5$ m/s, the warping constant $\lambda = 80\,\mathrm{eV}^3$, $\tau = 0.12$ ps, $\tau_\beta = 0.5$ ps, and $\Delta = 15$ meV.

where A and D encode the relative strength of phonon scattering versus spin-orbit and scalar disorder, respectively. The prefactors B and F depend on microscopic parameters such as the Fermi energy and gap. Using Eqs. (18) and (27), Fig. 3 shows $\chi_{xyy}(T)$ and its sensitivity to τ and τ_β, with the latter having stronger impact as it scales both contributions. In Fig. 4, we plot $\chi_{xyy}(T)$ varying the Fermi energy while keeping the relaxation times fixed. This behavior, observed in, e.g., Ref. [64], suggests skew scattering ($\sim\tau^3$) dominates. The subleading channel arises from a linear side-jump effect extended to second order, scaling as $\sim\tau$. These contributions have not been previously computed but become relevant at low Fermi energies, where interband coherence enhances quantum effects [85,86]. Our framework clarifies these mechanisms [87,88] and exposes the shortcomings of approximations that neglect their interplay.

Finally, we comment on the relation between the density-matrix formalism employed here and the semiclassical approach. In time-reversal-symmetric systems, the second-order response is known to exhibit a characteristic scaling with the relaxation time [8,37,89]. We emphasize, however, that from a microscopic perspective the physically meaningful parameter controlling disorder-induced relaxation is the impurity density. Indeed, relaxation processes originate from the imaginary part of the electronic self-energy, which changes sign under time-reversal symmetry. As a consequence, in time-reversal-broken systems the second-order current can only depend on even powers of disorder-induced relaxation processes. Beyond the first Born approximation, an additional characteristic time scale appears, associated with skew-scattering processes. Importantly, when the response is analyzed in terms of impurity density, this additional scale does not alter the fundamental scaling behavior of the nonlinear response. In this sense, both the semiclassical framework and the quantum Liouville approach predict qualitatively identical results. In experiments, nonlinear current measurements are typically normalized by the linear Drude-Boltzmann conductivity, which is insensitive to skew-scattering effects. As a result, the experimentally inferred scaling with the relaxation time may appear to contradict theoretical expectations. Our analysis clarifies that this apparent discrepancy arises from the choice of normalization rather than from a genuine difference between theoretical descriptions.

V. COMPARISON TO EXPERIMENTS

To analyze the way the nonlinear Hall response scales with disorder, a phenomenological scaling relation was proposed in Ref. [29] under the assumption of time-reversal symmetry. In that framework, linear scaling of the nonlinear Hall conductivity with the linear longitudinal conductivity was attributed to contributions from the BCD, side-jump, and skew-scattering mechanisms [90,91]. This approach was later adopted in experiments on the surface states of topological insulators [63], where a Berry curvature triple (BCT) was introduced as the driving mechanism behind the skew scattering—assumed to be constant—and associated with an overall scaling of order τ^3. Such an interpretation is consistent with systems that explicitly break $\mathcal{PT}$ symmetry. By contrast, the $\mathcal{PT}$-symmetric state studied in this work presents a fundamentally different scenario. In this case, the Berry curvature vanishes identically at each $\boldsymbol{k}$ due to symmetry, making the definition of a BCT ambiguous. This leaves disorder-induced mechanisms as the main source of nonlinear response. Our main result, Eq. (1), differs from the analysis in Ref. [63] in a crucial way: here, the skew scattering is not treated as a fixed or frozen quantity. Instead, both τ and τ_β are affected by temperature. This refinement is supported by recent experiments [39], which demonstrate that phonon interactions can influence skew scattering, aligning well with our theoretical predictions. Besides, Ref. [63] does not elaborate of the linear in τ contribution provided here, which is experimentally accessible.

The results presented in this work are derived within a well-defined regime of validity. First, we assume the quasiclassical limit $\hbar/\tau\varepsilon_F \ll 1$, which in Dirac materials is equivalent to $k_F l_0 \gg 1$, with l_0 the mean-free path. This allows for a controlled kinetic description in the well-known diffusive regime. Second, we focus on the high-temperature regime $T \gg T_{\mathrm{BG}}$, where electron-phonon scattering is quasielastic and can be consistently incorporated into the kinetic framework as an effective disorder channel via Matthiessen's rule. We recall that the Bloch-Gruneisen temperature is defined as $T_{\mathrm{BG}} = 2k_F v_{\mathrm{ph}}/k_B$, where v_{ph} is the sound velocity and k_B is the Boltzmann constant [54]. This regime is particularly

relevant for room-temperature experiments on topological materials. For topological materials such as Bi_2Te_3 Ref. [59] reported $T_{BG} = 3.9$ K, but this can vary depending on the sound velocity and Fermi wave vector. At lower temperatures, where different phonon modes, cooling mechanisms, or sample-specific effects become important—as is well known from studies of graphene and other Dirac systems—additional temperature ($\propto T^{-4}$ in the mobility) dependences may arise [57,92,93]. Such regimes lie beyond the scope of the present work. The temperature dependence shown in Figs. 3 and 4 is therefore not intended to imply quantitative validity across all temperature regimes. Rather, these figures are meant to illustrate the qualitative trends and crossovers that emerge from the competition between different disorder-driven contributions once phonon scattering becomes relevant. This perspective clarifies the range of applicability of our results and facilitates their comparison with experiments.

VI. CONCLUSION

We have studied the impact of disorder and phonon scattering on the nonlinear response of gapped topological insulators with hexagonal warping. Our formalism provides a consistent description of room-temperature experimental results, and shows that both skew-scattering and side-jump mechanisms make relevant contributions, even at subleading order. These results underscore the need for a careful treatment of relaxation processes beyond simplified models, and provide a versatile framework for other spin-orbit coupled systems and disorder scenarios.

DATA AVAILABILITY

There are no publicly available research data or software supporting this manuscript. Requests for further information or data should be sent to the authors.

APPENDIX A: REPRODUCING PREVIOUS RESULTS

Our approach is based on the solution of the quantum Liouville equation for the density matrix ρ, namely,

$$\frac{\partial \rho}{\partial t} + \frac{i}{\hbar}[H, \rho] = 0, \tag{A1}$$

where H is the Hamiltonian of the systems. In general, the Hamiltonian is written as $H = H_0 + H_E + U(\boldsymbol{r})$, where H_0 is the unperturbed band Hamiltonian, $H_E(\boldsymbol{r}) = e\boldsymbol{E}\cdot\boldsymbol{r}$ is the external driving term, and $U(\boldsymbol{r})$ is the disorder potential. The solution of the evolution equation for ρ follows straightforward steps described in Refs. [51,52]. First, we express the density matrix as $\rho \to \langle\rho\rangle + g$, where $\langle\rho\rangle$ is a disorder averaged part and g is a fluctuating part, which is off diagonal in momentum as will become clear with its definition below. Such a separation allows us to write a kinetic equation for $\langle\rho\rangle$, which reads

$$\frac{\partial \langle\rho\rangle}{\partial t} + \frac{i}{\hbar}[H_0, \langle\rho\rangle] + J_0(\langle\rho\rangle) = -\frac{i}{\hbar}[H_E, \langle\rho\rangle] - J_E(\langle\rho\rangle). \tag{A2}$$

The collision integrals $J_0(\langle\rho\rangle)$ and $J_E(\langle\rho\rangle)$ are defined through the fluctuating function g as $J_0(\langle\rho\rangle) = (i/\hbar)\langle[U, g_0]\rangle$ and $J_E(\langle\rho\rangle) = (i/\hbar)\langle[U, g_E]\rangle$ where

$$g_0 = \frac{1}{2\pi i}\int_{-\infty}^{\infty} d\epsilon G^R(\epsilon)[U, \langle\rho\rangle]G^A(\epsilon) \tag{A3}$$

$$g_E = \frac{1}{2\pi i}\int_{-\infty}^{\infty} d\epsilon G^R(\epsilon)[H_E, g_0]G^A(\epsilon) \tag{A4}$$

with $G^{R/A}(\epsilon)$ retarded and advanced free Green's functions [52] and $\langle\cdots\rangle$ means impurity average. Expressing the kinetic equation Eq. (A2) in the crystal momentum representation and changing $\langle\rho\rangle \to f_{\boldsymbol{k}}$ one can write

$$\frac{\partial f}{\partial t} + \frac{i}{\hbar}[H_0, f] + J_0(f) = \frac{e\boldsymbol{E}}{\hbar}\cdot\frac{Df}{D\boldsymbol{k}} - J_E(f), \tag{A5}$$

with the covariant derivative defined as $\frac{Df}{D\boldsymbol{k}} = \frac{df}{d\boldsymbol{k}} + i[f, \boldsymbol{\mathcal{R}}]$ where the Berry connection vector reads $\boldsymbol{\mathcal{R}}^{mm'} = i\langle u_{\boldsymbol{k}}^m|\boldsymbol{\nabla}_{\boldsymbol{k}}u_{\boldsymbol{k}}^{m'}\rangle$ and $|u_{\boldsymbol{k}}^{m'}\rangle$ are Bloch eigenstates of the unperturbed Hamiltonian.

In the main text we expressed the distribution as

$$f^{mm'} = n^{mm}\delta_{mm'} + S^{mm'}. \tag{A6}$$

The purpose of this notation is just to separate band diagonal/off-diagonal channels. In the stationary regime the off-diagonal $S^{mm'}$ follows from the equation

$$\frac{i}{\hbar}(\varepsilon_{m\boldsymbol{k}} - \varepsilon_{m'\boldsymbol{k}})S_E^{mn} = i\frac{eE_a}{\hbar}\left[n_E^m - n_E^{m'}\right]\mathcal{R}_a^{mm'}, \tag{A7}$$

which can be cast as

$$S_E^{mn} = eE_b\frac{\mathcal{R}_b^{mm'}}{(\varepsilon_{m\boldsymbol{k}} - \varepsilon_{m'\boldsymbol{k}})}\left(n_E^m - n_E^{m'}\right). \tag{A8}$$

To first order in the electric field the right-hand side should appear with the Fermi-Dirac distribution, namely, $n \to n_{\mathrm{FD}}(\varepsilon_{m\boldsymbol{k}})$. Hence

$$S_E^{mm'} = eE_b\frac{\mathcal{R}_b^{mm'}}{(\varepsilon_{m\boldsymbol{k}} - \varepsilon_{m'\boldsymbol{k}})}[n_{\mathrm{FD}}(\varepsilon_{m\boldsymbol{k}}) - n_{\mathrm{FD}}(\varepsilon_{m'\boldsymbol{k}})]. \tag{A9}$$

To second order in the electric field the right-hand side should appear with the linear response Boltzmann distribution, namely, $n \to n_E$, which in the relaxation time approximation is given by

$$n_E^{(-1)mm} = \tau\frac{e}{\hbar}\boldsymbol{E}\cdot\frac{\partial n_{\mathrm{FD}}\left(\varepsilon_{\boldsymbol{k}}^m\right)}{\partial\boldsymbol{k}} \tag{A10}$$

and the superscript in $n_E^{(-1)mm}$ meaning that it scales with inverse impurity density (linear in τ). Hence, to second order

$$S_{2E}^{mn} = eE_b\frac{\mathcal{R}_b^{mm'}}{(\varepsilon_{m\boldsymbol{k}} - \varepsilon_{m'\boldsymbol{k}})}\left[n_E^{(-1)mm} - n_E^{(-1)m'm'}\right]. \tag{A11}$$

This is the iterative procedure that we use in the main text to the full kinetic equation.

In order to reproduce the anomalous Hall effect, we take the off-diagonal velocity

$$v_a^{m'm} = i\hbar^{-1}(\varepsilon_{m'\boldsymbol{k}} - \varepsilon_{m\boldsymbol{k}})\mathcal{R}_a^{m'm} \tag{A12}$$

and trace it with the off-diagonal function $S_E^{mm'}$. We obtain

$$\sigma_{ab} = -e^2 \sum_{\boldsymbol{k}} \sum_{m} \sum_{m' \neq m} i\hbar^{-1}(\varepsilon_{m'\boldsymbol{k}} - \varepsilon_{m\boldsymbol{k}}) \mathcal{R}_a^{m'm} \times \frac{\mathcal{R}_b^{mm'}}{(\varepsilon_{m\boldsymbol{k}} - \varepsilon_{m'\boldsymbol{k}})} [n_{\mathrm{FD}}(\varepsilon_{m\boldsymbol{k}}) - n_{\mathrm{FD}}(\varepsilon_{m'\boldsymbol{k}})] \tag{A13}$$

$$= -\frac{e^2}{\hbar} i \sum_{\boldsymbol{k}} \sum_{m} \sum_{m' \neq m} \mathcal{R}_a^{m'm} \mathcal{R}_b^{mm'} [n_{\mathrm{FD}}(\varepsilon_{m\boldsymbol{k}}) - n_{\mathrm{FD}}(\varepsilon_{m'\boldsymbol{k}})]. \tag{A14}$$

Since all indexes are contracted, we can relabeled them so that the distribution is the common factor, namely

$$\sigma_{ab} = \frac{e^2}{\hbar} i \sum_{\boldsymbol{k}} \sum_{m} \sum_{m' \neq m} \left[\mathcal{R}_a^{mm'} \mathcal{R}_b^{m'm} - \mathcal{R}_a^{m'm} \mathcal{R}_b^{mm'}\right] n_{\mathrm{FD}}(\varepsilon_{m\boldsymbol{k}}). \tag{A15}$$

The Berry curvature of band m is identified as

$$\Omega_{ab}^{mm} = i \sum_{m' \neq m} \left[\mathcal{R}_a^{mm'} \mathcal{R}_b^{m'm} - \mathcal{R}_a^{m'm} \mathcal{R}_b^{mm'}\right]. \tag{A16}$$

Finally, we arrive at the equation of the anomalous Hall conductivity

$$\sigma_{ab} = \frac{e^2}{\hbar} \sum_{\boldsymbol{k}} \sum_{m} \Omega_{ab}^{mm} n_{\mathrm{FD}}(\varepsilon_{m\boldsymbol{k}}). \tag{A17}$$

In order to reproduce the nonlinear Berry curvature dipole, we follow similar steps. It is easy to show that the response is given by

$$\chi_{abc} = \frac{e^2}{\hbar} \sum_{\boldsymbol{k}} \sum_{m} \Omega_{ab}^{mm} n_{E_c}^{(-1)mm} \tag{A18}$$

$$= \tau \frac{e^3}{\hbar^2} \sum_{\boldsymbol{k}} \sum_{m} \Omega_{ab}^{mm} \frac{\partial n_{\mathrm{FD}}(\varepsilon_{\boldsymbol{k}}^m)}{\partial k_c} \tag{A19}$$

$$= -\tau \frac{e^3}{\hbar^2} \sum_{\boldsymbol{k}} \sum_{m} \frac{\partial \Omega_{ab}^{mm}}{\partial k_c} n_{\mathrm{FD}}(\varepsilon_{\boldsymbol{k}}^m), \tag{A20}$$

which is the response related to the Berry curvature dipole.

It is well known from semiclassic that the side-jump contribution arises when the work done by the electric field is incorporated in the semiclassical distribution. It leads to a shift in the energy given by

$$\delta W = -e\boldsymbol{E} \cdot \delta \boldsymbol{r}_{\boldsymbol{k},\boldsymbol{k}'}, \tag{A21}$$

which generates a driving term of the form $\propto -(\partial n_{\mathrm{FD}}/\partial \varepsilon) e\boldsymbol{E} \cdot \delta \boldsymbol{r}_{\boldsymbol{k},\boldsymbol{k}'}$, where

$$\delta \boldsymbol{r}_{\boldsymbol{k},\boldsymbol{k}'} = \boldsymbol{\mathcal{R}}_{\boldsymbol{k}'}^{mm} - \boldsymbol{\mathcal{R}}_{\boldsymbol{k}}^{mm} - \left(\frac{\partial}{\partial \boldsymbol{k}} + \frac{\partial}{\partial \boldsymbol{k}'}\right) arg\left(V_{\boldsymbol{k}',\boldsymbol{k}'}^{mm'}\right) \tag{A22}$$

and $V_{\boldsymbol{k}',\boldsymbol{k}'}^{mm'}$ are matrix elements of the scattering potential between Bloch states. The quantity $\delta \boldsymbol{r}_{\boldsymbol{k},\boldsymbol{k}'}$ is known as coordinates shift. In the present formalism this arises due to

$$J_E(\langle \rho \rangle) = (i/\hbar) \langle [U, g_E] \rangle. \tag{A23}$$

After projecting on to Bloch states we find

$$[J_E(n_{\mathrm{FD}})]_{\boldsymbol{k}}^{mm} = -\frac{2\pi}{\hbar} eE_i \sum_{\boldsymbol{k}'} \frac{\partial}{\partial \epsilon_{\boldsymbol{k}'}^m} \delta\left(\epsilon_{\boldsymbol{k}'}^m - \epsilon_{\boldsymbol{k}}^m\right) \left[n_{\mathrm{FD}}\left(\varepsilon_{\boldsymbol{k}'}^m\right) - n_{\mathrm{FD}}\left(\varepsilon_{\boldsymbol{k}}^m\right)\right] \times \mathrm{Im}\left\langle \left[\left(\frac{\partial}{\partial k_i'} + \frac{\partial}{\partial k_i}\right) U_{\boldsymbol{k}\boldsymbol{k}'}^{mm}\right] U_{\boldsymbol{k}'\boldsymbol{k}}^{mm} \right\rangle + \frac{2\pi}{\hbar} eE_i \sum_{\boldsymbol{k}'} \frac{\partial}{\partial \epsilon_{\boldsymbol{k}'}^m} \delta\left(\epsilon_{\boldsymbol{k}'}^m - \epsilon_{\boldsymbol{k}}^m\right) \left(\mathcal{R}_{\boldsymbol{k},i}^{mm} - \mathcal{R}_{\boldsymbol{k}',i}^{mm}\right) \times \left[n_{\mathrm{FD}}\left(\varepsilon_{\boldsymbol{k}'}^m\right) - n_{\mathrm{FD}}\left(\varepsilon_{\boldsymbol{k}}^m\right)\right] \langle U_{\boldsymbol{k}\boldsymbol{k}'}^{mm} U_{\boldsymbol{k}'\boldsymbol{k}}^{mm} \rangle. \tag{A24}$$

The similarity with the coordinate shift is apparent. When the coordinates shift is properly incorporated into the semiclassical formalism it can be shown that both formalism reproduced the same result [52,66–68].

APPENDIX B: LEADING LINEAR RESPONSE: BOLTZMANN

The band diagonal elements of the kinetic equation leads to the Boltzmann equation, namely,

$$\left[J\left(n_E^{(-1)}\right)\right]_{\boldsymbol{k}}^{mm} = \frac{e}{\hbar} \boldsymbol{E} \cdot \frac{\partial n_{\mathrm{FD}}\left(\varepsilon_{\boldsymbol{k}}^m\right)}{\partial \boldsymbol{k}}. \tag{B1}$$

The term to the right is the driving term and Eq. (B1) will provide the leading-order linear response distribution. We need to find the driving term up to linear order in the warping parameter. To this end, we expand the equilibrium Fermi-Dirac distribution to first order in the warping parameter, namely

$$n_{\mathrm{FD}}\left(\varepsilon_{\boldsymbol{k}}^m\right) = n_{\mathrm{FD}}\left(\varepsilon_{0\boldsymbol{k}}^m\right) + \lambda \frac{\partial \varepsilon_{\boldsymbol{k}}^m}{\partial \lambda} \frac{\partial n_{\mathrm{FD}}\left(\varepsilon_{0\boldsymbol{k}}^m\right)}{\partial \varepsilon_{0\boldsymbol{k}}^m}. \tag{B2}$$

In the presence of the warping term, the energy of the system is anisotropic. It reads

$$\varepsilon_{\boldsymbol{k}} = \sqrt{\hbar^2 v_F^2 k_x^2 + \hbar^2 v_F^2 k_y^2 + \left(\Delta + \frac{\lambda}{2}(k_+^3 + k_-^3)\right)^2}. \tag{B3}$$

We expand the energy in terms of the warping parameter. Then we can write the dispersion relation up to first order in the warping parameter as

$$\varepsilon_{\boldsymbol{k}} \approx \varepsilon_{0\boldsymbol{k}} + \lambda \xi_{0\boldsymbol{k}} k^3 \cos(3\theta_{\boldsymbol{k}}). \tag{B4}$$

This expansion will be very important for the rest of our procedure. The Fermi-Dirac distribution function then reads

$$n_{\mathrm{FD}}\left(\varepsilon_{\boldsymbol{k}}^m\right) \approx n_{\mathrm{FD}}\left(\varepsilon_{0\boldsymbol{k}}^m\right) + \lambda \xi_{0\boldsymbol{k}} k^3 \cos(3\theta_{\boldsymbol{k}}) \frac{\partial n_{\mathrm{FD}}\left(\varepsilon_{0\boldsymbol{k}}^m\right)}{\partial \varepsilon_{0\boldsymbol{k}}^m}. \tag{B5}$$

Now we can calculate the driving term in Eq. (B1). For the partial derivative we use polar coordinates, namely

$$\frac{\partial}{\partial k_x} = \cos(\theta_{\boldsymbol{k}}) \frac{\partial}{\partial k} - \frac{1}{k} \sin(\theta_{\boldsymbol{k}}) \frac{\partial}{\partial \theta_{\boldsymbol{k}}} \tag{B6}$$

$$\frac{\partial}{\partial k_y} = \sin(\theta_{\boldsymbol{k}}) \frac{\partial}{\partial k} + \frac{1}{k} \cos(\theta_{\boldsymbol{k}}) \frac{\partial}{\partial \theta_{\boldsymbol{k}}}. \tag{B7}$$

The linear response distributions then follow as

$$n^{(-1)}_{Ex\boldsymbol{k}} = \tau\frac{e}{\hbar}E_x\frac{\partial n_{\rm FD}\left(\varepsilon^m_{0\boldsymbol{k}}\right)}{\partial k_x} \tag{B8}$$

$$+\tau\lambda\frac{e}{\hbar}E_x\cos(\theta_{\boldsymbol{k}})\cos(3\theta_{\boldsymbol{k}})\frac{\partial}{\partial k}\left(\xi_{0\boldsymbol{k}}k^3\frac{\partial n_{\rm FD}\left(\varepsilon^m_{0\boldsymbol{k}}\right)}{\partial\varepsilon^m_{0\boldsymbol{k}}}\right) \tag{B9}$$

$$+\tau 3\lambda\frac{e}{\hbar}E_x\frac{1}{k}\sin(\theta_{\boldsymbol{k}})\sin(3\theta_{\boldsymbol{k}})\xi_{0\boldsymbol{k}}k^3\frac{\partial n_{\rm FD}\left(\varepsilon^m_{0\boldsymbol{k}}\right)}{\partial\varepsilon^m_{0\boldsymbol{k}}}, \tag{B10}$$

$$n^{(-1)}_{Ey\boldsymbol{k}} = \tau\frac{e}{\hbar}E_y\frac{\partial n_{\rm FD}\left(\varepsilon^m_{0\boldsymbol{k}}\right)}{\partial k_y} \tag{B11}$$

$$+\tau\lambda\frac{e}{\hbar}E_y\sin(\theta_{\boldsymbol{k}})\cos(3\theta_{\boldsymbol{k}})\frac{\partial}{\partial k}\left(\xi_{0\boldsymbol{k}}k^3\frac{\partial n_{\rm FD}\left(\varepsilon^m_{0\boldsymbol{k}}\right)}{\partial\varepsilon^m_{0\boldsymbol{k}}}\right) \tag{B12}$$

$$-\tau 3\lambda\frac{e}{\hbar}E_y\frac{1}{k}\cos(\theta_{\boldsymbol{k}})\sin(3\theta_{\boldsymbol{k}})\xi_{0\boldsymbol{k}}k^3\frac{\partial n_{\rm FD}\left(\varepsilon^m_{0\boldsymbol{k}}\right)}{\partial\varepsilon^m_{0\boldsymbol{k}}}. \tag{B13}$$

So far, we have calculated the linear response distribution, necessary to calculate the nonlinear response.

APPENDIX C: NONLINEAR DISTRIBUTION: LEADING RESPONSE COEFFICIENT

In this section we explain the main steps to calculate the nonlinear distributions. Such a distribution will provide the second-order response $\chi_{xyy} = \chi^{(2)}_{xyy} + \chi^{(0)}_{xyy}$ of the systems. The coefficient $\chi^{(2)}_{xyy}$ is the leading-order contribution, which scales with impurity density as $\sim n^{-2}_{\rm imp}$ but is the result of the ration of two different relaxation processes $\chi^{(2)}_{xyy} \sim (1/\tau_\beta)/(1/\tau^3)$ both scaling linear in impurity density. The subleading response is independent of impurity density but it is the result of the scaling of two relaxation processes namely $\chi^{(0)}_{xyy} \sim (1/\tau_\beta)/(1/\tau)$.

The leading-order nonlinear distribution satisfies the kinetic equation

$$\left[J_0\left(n^{(-2)}_{E2}\right)\right]^{mm}_{\boldsymbol{k}} = \frac{e\boldsymbol{E}}{\hbar}\cdot\frac{\partial}{\partial\boldsymbol{k}}n^{(-1)mm}_{E\boldsymbol{k}}. \tag{C1}$$

For simplicity, we will use the relaxation time approximation. In this case we take $[J_0(n^{(-2)}_{E2})]^{mm}_{\boldsymbol{k}} = n^{(-2)mm}_{E2}/\tau$, where τ is the relaxation time. In order to calculate the driving term, we need to take the derivatives of the linear response function $n^{(-1)mm}_{E\boldsymbol{k}}$. We are mostly interested in a transversal current such as $j_x \propto E_yE_y$. Then, we will use the linear response $n^{(-1)}_{Ey\boldsymbol{k}}$ to calculate the leading-order nonlinear distribution $n^{(-2)}_{EyEy\boldsymbol{k}}$. We again use polar coordinates. The distribution reads

$$n^{(-2)}_{EyEy\boldsymbol{k}} = \tau^2\frac{e}{\hbar}E_y\frac{e}{\hbar}E_y\frac{\partial n_{\rm FD}\left(\varepsilon^m_{0\boldsymbol{k}}\right)}{\partial k_y} + \tau^2\frac{e}{\hbar}E_y\lambda\frac{e}{\hbar}E_y\sin^2(\theta_{\boldsymbol{k}})\cos(3\theta_{\boldsymbol{k}})\frac{\partial^2}{\partial k^2}\left(\xi_{0\boldsymbol{k}}k^3\frac{\partial n_{\rm FD}\left(\varepsilon^m_{0\boldsymbol{k}}\right)}{\partial\varepsilon^m_{0\boldsymbol{k}}}\right) - \tau^2\frac{e}{\hbar}E_y3\lambda\frac{e}{\hbar}E_y\sin(\theta_{\boldsymbol{k}})\cos(\theta_{\boldsymbol{k}})\sin(3\theta_{\boldsymbol{k}})$$
$$\times\ \frac{\partial}{\partial k}\left(\xi_{0\boldsymbol{k}}k^2\frac{\partial n_{\rm FD}\left(\varepsilon^m_{0\boldsymbol{k}}\right)}{\partial\varepsilon^m_{0\boldsymbol{k}}}\right) + \tau^2\frac{e}{\hbar}E_y\lambda\frac{e}{\hbar}E_y\frac{1}{k}\cos(\theta_{\boldsymbol{k}})[\cos(\theta_{\boldsymbol{k}})\cos(3\theta_{\boldsymbol{k}}) - 3\sin(\theta_{\boldsymbol{k}})\sin(3\theta_{\boldsymbol{k}})]$$
$$\times\ \frac{\partial}{\partial k}\left(\xi_{0\boldsymbol{k}}k^3\frac{\partial n_{\rm FD}\left(\varepsilon^m_{0\boldsymbol{k}}\right)}{\partial\varepsilon^m_{0\boldsymbol{k}}}\right) - \tau^2\frac{e}{\hbar}E_y3\lambda\frac{e}{\hbar}E_y\frac{1}{k}\cos(\theta_{\boldsymbol{k}})[-\sin(\theta_{\boldsymbol{k}})\sin(3\theta_{\boldsymbol{k}}) + 3\cos(\theta_{\boldsymbol{k}})\cos(3\theta_{\boldsymbol{k}})]\left(\xi_{0\boldsymbol{k}}k^2\frac{\partial n_{\rm FD}\left(\varepsilon^m_{0\boldsymbol{k}}\right)}{\partial\varepsilon^m_{0\boldsymbol{k}}}\right). \tag{C2}$$

The leading-order distribution $n^{(-2)}_{EyEy\boldsymbol{k}}$ allows us to compute a renormalized distribution in order to take into account extrinsic skew-scattering events. We will calculate such a distribution in the following section.

1. Calculating the renormalized leading-order distribution: β-dependent diagonal distribution

In this section we calculate the renormalized distribution $n^{(-2)++}_{EyEy\beta}$, which produces a transversal current such as $j_x = \chi^{(-2)}_{xyy}E_yE_y$. Once we calculate the distribution $n^{(-2)}_{E2\boldsymbol{k}}$ we can use it to generate a new driving term. This follows from the collision integral of extrinsic spin-orbit scattering. Then, we want to solve the kinetic equation

$$\left[J_0\left(n^{(-2)}_{E2,\beta}\right)\right]^{mm}_{\boldsymbol{k}} = -\left[J_\beta\left(n^{(-2)}_{E2}\right)\right]^{mm}_{\boldsymbol{k}}, \tag{C3}$$

where the right-hand side is a driving term. The notation related to β means that we use extrinsic spin-orbit scattering events. The diagonal collision integral as a function of a diagonal distribution reads

$$\left[J_\beta\left(n^{(-2)}_{E2}\right)\right]^{mm}_{\boldsymbol{k}} = \frac{2\pi}{\hbar}\sum_{\boldsymbol{k}'}\left\langle U^{mm}_{\boldsymbol{k}\boldsymbol{k}'}U^{mm}_{\boldsymbol{k}'\boldsymbol{k}}\right\rangle_\beta\left(n^{(-2)mm}_{E\boldsymbol{k}} - n^{(-2)mm}_{E\boldsymbol{k}'}\right)\delta\left(\epsilon^m_{\boldsymbol{k}} - \epsilon^m_{\boldsymbol{k}'}\right), \tag{C4}$$

where $n^{(-2)mm}_{E\boldsymbol{k}}$ is already known. For the scattering events we need the matrix elements

$$\langle U^{++}_{\boldsymbol{k}\boldsymbol{k}'}U^{++}_{\boldsymbol{k}'\boldsymbol{k}}\rangle = u_0^2\beta^2(kk')^2\sin^2(\theta_{\boldsymbol{k}} - \theta_{\boldsymbol{k}'})\tfrac{1}{2}\left[1 + \xi_k\xi_{k'} - \left(1-\xi_k^2\right)^{1/2}\left(1-\xi_{k'}^2\right)^{1/2}\cos(\theta_{\boldsymbol{k}} - \theta_{\boldsymbol{k}'})\right]. \tag{C5}$$

Using the relaxation time approximation, namely, $n^{(-2)mm}_{E2,\beta}/\tau = -[J_\beta(n^{(-2)}_E)]^{mm}_{\boldsymbol{k}}$ we get

$$\begin{aligned}
\big[n^{(-2)}_{E_yE_y\boldsymbol{k}}\big]_\beta =& -\frac{\tau^3}{\tau_\beta}\frac{1}{2}\big[1+\xi_k^2\big]\Big(\frac{e}{\hbar}E_y\lambda\frac{e}{\hbar}E_y\Big)\sin^2(\theta_{\boldsymbol{k}})\cos(3\theta_{\boldsymbol{k}})\frac{\partial^2}{\partial k^2}\left(\xi_{0\boldsymbol{k}}k^3\frac{\partial n_{\rm FD}\big(\varepsilon^m_{0\boldsymbol{k}}\big)}{\partial\varepsilon^m_{0\boldsymbol{k}}}\right)\\
&+\frac{\tau^3}{\tau_\beta}\frac{1}{2}\big[1+\xi_k^2\big]\Big(\frac{e}{\hbar}E_y3\lambda\frac{e}{\hbar}E_y\Big)\sin(\theta_{\boldsymbol{k}})\cos(\theta_{\boldsymbol{k}})\sin(3\theta_{\boldsymbol{k}})\frac{\partial}{\partial k}\left(\xi_{0\boldsymbol{k}}k^2\frac{\partial n_{\rm FD}\big(\varepsilon^m_{0\boldsymbol{k}}\big)}{\partial\varepsilon^m_{0\boldsymbol{k}}}\right)\\
&-\frac{\tau^3}{\tau_\beta}\frac{1}{2}\big[1+\xi_k^2\big]\Big(\frac{e}{\hbar}E_y\lambda\frac{e}{\hbar}E_y\Big)\frac{1}{k}\cos(\theta_{\boldsymbol{k}})[\cos(\theta_{\boldsymbol{k}})\cos(3\theta_{\boldsymbol{k}})-3\sin(\theta_{\boldsymbol{k}})\sin(3\theta_{\boldsymbol{k}})]\frac{\partial}{\partial k}\left(\xi_{0\boldsymbol{k}}k^3\frac{\partial n_{\rm FD}\big(\varepsilon^m_{0\boldsymbol{k}}\big)}{\partial\varepsilon^m_{0\boldsymbol{k}}}\right)\\
&+\frac{\tau^3}{\tau_\beta}\frac{1}{2}\big[1+\xi_k^2\big]\Big(\frac{e}{\hbar}E_y3\lambda\frac{e}{\hbar}E_y\Big)\frac{1}{k}\cos(\theta_{\boldsymbol{k}})[-\sin(\theta_{\boldsymbol{k}})\sin(3\theta_{\boldsymbol{k}})+3\cos(\theta_{\boldsymbol{k}})\cos(3\theta_{\boldsymbol{k}})]\xi_{0\boldsymbol{k}}k^2\frac{\partial n_{\rm FD}\big(\varepsilon^m_{0\boldsymbol{k}}\big)}{\partial\varepsilon^m_{0\boldsymbol{k}}}\\
&+\frac{\tau^3}{\tau_\beta}\Big[\frac{e}{\hbar}E_y\lambda\frac{e}{\hbar}E_y\Big]\Big[\frac{1}{32}\Big][-\cos(\theta_{\boldsymbol{k}})-2\cos(3\theta_{\boldsymbol{k}})]\big[-\big(1-\xi_k^2\big)^{1/2}\big(1-\xi_k^2\big)^{1/2}\big]\frac{\partial^2}{\partial k^2}\left(\xi_{0\boldsymbol{k}'}k^3\frac{\partial n_{\rm FD}\big(\varepsilon^m_{0\boldsymbol{k}}\big)}{\partial\varepsilon^m_{0\boldsymbol{k}}}\right)\\
&-\frac{\tau^3}{\tau_\beta}\Big[\frac{e}{\hbar}E_y3\lambda\frac{e}{\hbar}E_y\Big]\Big[\frac{1}{32}\Big][\cos(\theta_{\boldsymbol{k}})]\big[-\big(1-\xi_k^2\big)^{1/2}\big(1-\xi_k^2\big)^{1/2}\big]\frac{\partial}{\partial k}\left(\xi_{0\boldsymbol{k}}k^2\frac{\partial n_{\rm FD}\big(\varepsilon^m_{0\boldsymbol{k}}\big)}{\partial\varepsilon^m_{0\boldsymbol{k}}}\right)\\
&+\frac{\tau^3}{\tau_\beta}\Big[\frac{e}{\hbar}E_y\lambda\frac{e}{\hbar}E_y\Big]\frac{1}{k}\Big[\frac{1}{16}\Big][-\cos(\theta_{\boldsymbol{k}})-\cos(3\theta_{\boldsymbol{k}})]\big[-\big(1-\xi_k^2\big)^{1/2}\big(1-\xi_k^2\big)^{1/2}\big]\frac{\partial}{\partial k}\left(\xi_{0\boldsymbol{k}}k^3\frac{\partial n_{\rm FD}\big(\varepsilon^m_{0\boldsymbol{k}}\big)}{\partial\varepsilon^m_{0\boldsymbol{k}}}\right)\\
&-\frac{\tau^3}{\tau_\beta}\Big[\frac{e}{\hbar}E_y3\lambda\frac{e}{\hbar}E_y\Big]\frac{1}{k}\Big[\frac{1}{16}\Big][\cos(\theta_{\boldsymbol{k}})-3\cos(3\theta_{\boldsymbol{k}})]\big[-\big(1-\xi_k^2\big)^{1/2}\big(1-\xi_k^2\big)^{1/2}\big]\left(\xi_{0\boldsymbol{k}}k^2\frac{\partial n_{\rm FD}\big(\varepsilon^m_{0\boldsymbol{k}}\big)}{\partial\varepsilon^m_{0\boldsymbol{k}}}\right).
\end{aligned}\tag{C6}$$

We defined a constant relaxation time due to extrinsic spin-orbit coupling in impurity scattering as $\gamma_\beta = 1/\tau_\beta = \pi\rho(\epsilon_F)[u_0^2\beta^2(k_F)^4]/\hbar$. The current follows as $\langle j_x\rangle = -e\mathrm{Tr}[v_x[n^{(-2)}_{E_yE_y\boldsymbol{k}}]_\beta]$, which can be written as $\langle j_x\rangle = \chi^{(-2)}_{xyy}E_yE_y$, with the transversal response $\chi^{(-2)}_{xyy}$. After a some algebra we find

$$\big[\chi^{(-2)}_{xyy}\big]_\beta = \lambda\gamma_\beta\tau^3\Big(\frac{e}{\hbar}\Big)^3\Big(\frac{1}{64}\Big)\rho(\epsilon_{\boldsymbol{k}})\big(1-\xi_F^2\big)(\xi_F\varepsilon_F)\big[15+13\xi_F^2-75\xi_F^4+33\xi_F^6\big].\tag{C7}$$

This provide the leading renormalized second-order response. In the following we will calculate the subleading renormalized second-order response.

APPENDIX D: NONLINEAR DISTRIBUTION: SUBLEADING RESPONSE

In this section we calculate the distribution functions that leads to the response $\chi^{(0)}_{xyy}$. This is mainly the result of side-jump and skew-scattering nonlinear events that have roots on a linear side-jump effect. This is explained in this way: as for the leading-order response, the subleading second-order response depends on a previous subleading linear distribution. Such a subleading linear distribution is related to a side-jump effect. Then, based on a linear side-jump effect, we will define nonlinear side-jump and skew-scattering contributions. In the following we will show the main steps of our theoretical approach.

1. Subleading β-renormalized side-jump effect

In this section we calculate the subleading β-dependent side-jump effect. To this end, we first need to work out some terms related to linear response regime. Our first step is to solve the kinetic equation

$$\big[J_0\big(n^{(0)}_{E,\beta}\big)\big]^{mm}_{\boldsymbol{k}} = -\big[J_{E,\beta}\big(n^{(0)}_{\rm FD}\big)\big]^{mm}_{\boldsymbol{k}},\tag{D1}$$

which will provide the linear response distribution $n^{(0)}_{E,\beta}$.

A general expression for the electric field corrected collision integral up to first order is

$$\begin{aligned}
[J_E(n_{\rm FD})]^{mm}_{\boldsymbol{k}} =& -\frac{2\pi}{\hbar}eE_i\sum_{\boldsymbol{k}'}\frac{\partial}{\partial\epsilon^m_{\boldsymbol{k}'}}\delta\big(\epsilon^m_{\boldsymbol{k}'}-\epsilon^m_{\boldsymbol{k}}\big)\big[n_{\rm FD}\big(\varepsilon^m_{\boldsymbol{k}'}\big)-n_{\rm FD}\big(\varepsilon^m_{\boldsymbol{k}}\big)\big]\,\mathrm{Im}\left\langle\left[\left(\frac{\partial}{\partial k'_i}+\frac{\partial}{\partial k_i}\right)U^{mm}_{\boldsymbol{k}\boldsymbol{k}'}\right]U^{mm}_{\boldsymbol{k}'\boldsymbol{k}}\right\rangle\\
&+\frac{2\pi}{\hbar}eE_i\sum_{\boldsymbol{k}'}\frac{\partial}{\partial\epsilon^m_{\boldsymbol{k}'}}\delta\big(\epsilon^m_{\boldsymbol{k}'}-\epsilon^m_{\boldsymbol{k}}\big)\big(\mathcal{R}^{mm}_{\boldsymbol{k},i}-\mathcal{R}^{mm}_{\boldsymbol{k}',i}\big)\big[n_{\rm FD}\big(\varepsilon^m_{\boldsymbol{k}'}\big)-n_{\rm FD}\big(\varepsilon^m_{\boldsymbol{k}}\big)\big]\big\langle U^{mm}_{\boldsymbol{k}\boldsymbol{k}'}U^{mm}_{\boldsymbol{k}'\boldsymbol{k}}\big\rangle.
\end{aligned}\tag{D2}$$

We use the extrinsic spin orbit scattering potential in the above expression in the second line, namely

$$\left\langle U^{mm}_{\boldsymbol{k}\boldsymbol{k}'} U^{mm}_{\boldsymbol{k}'\boldsymbol{k}} \right\rangle_\beta = u_0^2 \beta^2 (kk')^2 \sin^2(\theta_{\boldsymbol{k}} - \theta_{\boldsymbol{k}'}) [\sigma_z]^{mm}_{\boldsymbol{k}\boldsymbol{k}'} [\sigma_z]^{mm}_{\boldsymbol{k}'\boldsymbol{k}}. \tag{D3}$$

Since we are interested in the distribution proportional to E_y, then we can use the Berry connection $\mathcal{R}^{++}_{\boldsymbol{k},y} = \frac{1}{2}(1+\xi_k)\frac{1}{k}\cos(\theta)$. With the equation $[J(n^{(0)}_{E,\beta})]^{++}_{\boldsymbol{k}} = -[J_{E,\beta}(n_{\mathrm{FD}})]^{++}_{\boldsymbol{k}}$ we find in the relaxation time approximation a side-jump-like distribution of the form

$$n^{(0)++}_{E,\beta} = -\frac{\lambda}{16} e E_y \tau \gamma_\beta A_{\boldsymbol{k}} \cos(2\theta_{\boldsymbol{k}}) - \frac{\lambda}{16} e E_y \tau \gamma_\beta B_{\boldsymbol{k}} \cos(\theta_{\boldsymbol{k}}) \cos(3\theta_{\boldsymbol{k}}) - \frac{\lambda}{16} e E_y \tau \gamma_\beta C_{\boldsymbol{k}} \sin(\theta_{\boldsymbol{k}}) \sin(3\theta_{\boldsymbol{k}}). \tag{D4}$$

The coefficients are

$$A_k = \left(\frac{\xi^2_{0\boldsymbol{k}} \varepsilon_{\boldsymbol{k}}}{\hbar^2 v_F^2}\right)\left(1+3\xi_k^2\right)\left(1-\xi_k^2\right)\delta(\varepsilon_{\boldsymbol{k}} - \varepsilon_F) + \left(\frac{\xi^2_{0\boldsymbol{k}} \varepsilon^2_{\boldsymbol{k}}}{\hbar^2 v_F^2}\right)\left(1-\xi_k^2\right)^2 \frac{\partial}{\partial \epsilon_{\boldsymbol{k}}}\delta(\varepsilon_{\boldsymbol{k}} - \varepsilon_F) \tag{D5}$$

$$\begin{aligned} B_k = {} & \left[-\xi_k\left(1-\xi_k^2\right)\right]\left[\xi_{0\boldsymbol{k}} k^2 \frac{\partial}{\partial \epsilon_{\boldsymbol{k}}}\delta(\varepsilon_{\boldsymbol{k}} - \varepsilon_F)\right] + \left[3\left(1-\xi_k^2\right)^{3/2}\right]\left[\xi_k^3 + \left(1-\xi_k^2\right)(-2\xi_k)\right] \\ & \times \left[\frac{\xi_{0\boldsymbol{k}}\varepsilon_{\boldsymbol{k}}}{\hbar^2 v_F^2}\delta(\varepsilon_{\boldsymbol{k}} - \varepsilon_F)\right] + \left[-4\xi_k^3\right]\left[\frac{\xi_{0\boldsymbol{k}}\varepsilon_{\boldsymbol{k}}}{\hbar^2 v_F^2}\left(1-\xi_k^2\right)\delta(\varepsilon_{\boldsymbol{k}} - \varepsilon_F)\right] \end{aligned} \tag{D6}$$

$$C_k = -2\frac{\xi^2_{0\boldsymbol{k}}\varepsilon_{\boldsymbol{k}}}{\hbar^2 v_F^2}\left(1+\xi_k^2\right)\left(1-\xi_k^2\right)^{3/2}\delta(\varepsilon_{\boldsymbol{k}} - \varepsilon_F) - \frac{\xi^2_{0\boldsymbol{k}}\varepsilon^2_{\boldsymbol{k}}}{\hbar^2 v_F^2}\left(1-\xi_k^2\right)^{5/2}\frac{\partial}{\partial \varepsilon_{\boldsymbol{k}}}\delta(\varepsilon_{\boldsymbol{k}} - \varepsilon_F). \tag{D7}$$

2. β-renormalized nonlinear diagonal distribution

With the linear distribution $n^{(0)}_{E,\beta}$ we can find the nonlinear distribution $n^{(-1)}_{E2,\beta}$. In the nonlinear regime we need to solve the kinetic equation

$$\left[J_0\left(n^{(-1)}_{E2,\beta}\right)\right]^{mm}_{\boldsymbol{k}} = \frac{n^{(-1)}_{E2,\beta}}{\tau} = \frac{e\boldsymbol{E}}{\hbar}\cdot\frac{\partial n^{(0)}_{E,\beta}}{\partial \boldsymbol{k}}. \tag{D8}$$

Using the derivative in polar coordinates we find

$$\begin{aligned} n^{(-1)}_{E2,\beta} = {} & -\frac{\lambda}{16}\frac{e^2E_y^2}{\hbar}\tau^2\gamma_\beta\left[\sin(\theta_{\boldsymbol{k}})\cos(2\theta_{\boldsymbol{k}})\frac{\partial}{\partial k}A_{\boldsymbol{k}} - A_{\boldsymbol{k}}\frac{1}{k}2\cos(\theta_{\boldsymbol{k}})\sin(2\theta_{\boldsymbol{k}})\right] \\ & -\frac{\lambda}{16}\frac{e^2E_y^2}{\hbar}\tau^2\gamma_\beta\left[\sin(\theta_{\boldsymbol{k}})\cos(\theta_{\boldsymbol{k}})\cos(3\theta_{\boldsymbol{k}})\frac{\partial}{\partial k}B_{\boldsymbol{k}} - B_{\boldsymbol{k}}\frac{1}{k}\cos(\theta_{\boldsymbol{k}})[\sin(\theta_{\boldsymbol{k}})\cos(3\theta_{\boldsymbol{k}}) + 3\cos(\theta_{\boldsymbol{k}})\sin(3\theta_{\boldsymbol{k}})]\right] \\ & -\frac{\lambda}{16}\frac{e^2E_y^2}{\hbar}\tau^2\gamma_\beta\left[\sin(\theta_{\boldsymbol{k}})\sin(\theta_{\boldsymbol{k}})\sin(3\theta_{\boldsymbol{k}})\frac{\partial}{\partial k}C_{\boldsymbol{k}} + C_{\boldsymbol{k}}\frac{1}{k}\cos(\theta_{\boldsymbol{k}})[\cos(\theta_{\boldsymbol{k}})\sin(3\theta_{\boldsymbol{k}}) + 3\sin(\theta_{\boldsymbol{k}})\cos(3\theta_{\boldsymbol{k}})]\right]. \end{aligned} \tag{D9}$$

Now, we use the off-diagonal velocity $v_x^{mm'} = i\hbar^{-1}(\varepsilon^m_{\boldsymbol{k}} - \varepsilon^{m'}_{\boldsymbol{k}})\mathcal{R}_x^{mm'}$ and the off-diagonal density matrix

$$S^{(0)mm'}_{E2\boldsymbol{k},\beta} = -\frac{\hbar}{i\left(\epsilon^m_{\boldsymbol{k}} - \epsilon^{m'}_{\boldsymbol{k}}\right)}\left[J_0\left(n^{(-1)}_{E2,\beta}\right)\right]^{mm'}_{\boldsymbol{k}}. \tag{D10}$$

The current can be written in the form

$$j_x = -e\sum_{\boldsymbol{k}} n^{(-1)++}_{E2,\beta} v^{++}_{\mathrm{ext},x}, \tag{D11}$$

where the extrinsic velocity is $v^{++}_{\mathrm{ext},x} = -\frac{1}{\tau}\frac{\hbar}{\varepsilon_k}\xi_k(1-\xi_k^2)^{1/2}v_F\sin(\theta_{\boldsymbol{k}})$. This gives the response

$$\left[\chi^{(0)}_{xyy}\right]_{sj} = -\lambda\frac{e^3}{\hbar}\frac{\tau}{\tau_\beta}\frac{\rho(\varepsilon_F)}{\varepsilon_F}\xi_F^3\left(1-\xi_F^2\right)\frac{1}{128}\left\{\left(1-\xi_F^2\right)\left[\left(16-18\xi_F^2\right)\right] + \left(1-\xi_F^2\right)^{1/2}\left[-22+32\xi_F^2-6\xi_F^4\right]\right\}. \tag{D12}$$

3. β-renormalized nonlinear off-diagonal distribution: First contribution

In order to calculate the skew scattering, it is necessary to calculate the explicit off-diagonal distribution. Namely, we need to calculate the distribution

$$S^{(0)mm'}_{E2\boldsymbol{k},\beta} = -\frac{\hbar}{i\big(\epsilon^m_{\boldsymbol{k}} - \epsilon^{m'}_{\boldsymbol{k}}\big)}\big[J_0\big(n^{(-1)}_{E2,\beta}\big)\big]^{mm'}_{\boldsymbol{k}}. \tag{D13}$$

Basically we need $n^{(-1)}_{E2,\beta}$ and the equation

$$\big[J\big(n^{(-1)}_{E2,\beta}\big)\big]^{+-}_{\boldsymbol{k}} = \frac{\pi}{\hbar}\sum_{\boldsymbol{k}'}\langle U^{++}_{\boldsymbol{k},\boldsymbol{k}'}U^{+-}_{\boldsymbol{k}',\boldsymbol{k}}\rangle\big(n^{(-1)++}_{E2\boldsymbol{k},\beta} - n^{(-1)++}_{E2\boldsymbol{k}',\beta}\big)\delta(\epsilon^+_{\boldsymbol{k}'} - \epsilon^+_{\boldsymbol{k}}) \tag{D14}$$

$$= \frac{\pi}{\hbar}\big(n^{(-1)++}_{E2\boldsymbol{k},\beta}\big)\sum_{\boldsymbol{k}'}\langle U^{++}_{\boldsymbol{k},\boldsymbol{k}'}U^{+-}_{\boldsymbol{k}',\boldsymbol{k}}\rangle\delta(\epsilon^+_{\boldsymbol{k}'} - \epsilon^+_{\boldsymbol{k}}) + \frac{\pi}{\hbar}\sum_{\boldsymbol{k}'}\langle U^{++}_{\boldsymbol{k},\boldsymbol{k}'}U^{+-}_{\boldsymbol{k}',\boldsymbol{k}}\rangle\big(-n^{(-1)++}_{E2\boldsymbol{k}',\beta}\big)\delta(\epsilon^+_{\boldsymbol{k}'} - \epsilon^+_{\boldsymbol{k}}). \tag{D15}$$

$$\begin{aligned}
S^{(0)+-}_{E2\boldsymbol{k},\beta} = {} & i\frac{\hbar}{4\varepsilon_{\boldsymbol{k}}}\frac{1}{\tau}\big(n^{(-1)++}_{E2\boldsymbol{k},\beta}\big)\big[\xi_k\big(1-\xi_k^2\big)^{1/2}\big] - \frac{\hbar}{4\varepsilon_{\boldsymbol{k}}}\frac{1}{\tau}\bigg(-\frac{\lambda}{16}\frac{e^2E_y^2}{\hbar}\tau^2\gamma_\beta\bigg)\bigg[\bigg(\frac{1}{4}\bigg)\frac{\partial}{\partial k}A_{\boldsymbol{k}} + \bigg(\frac{1}{2}\bigg)\frac{1}{k}A_{\boldsymbol{k}}\bigg]\big[i\xi_k\big(1-\xi_k^2\big)^{1/2}\sin(\theta_{\boldsymbol{k}})\big] \\
& - \frac{\hbar}{4\varepsilon_{\boldsymbol{k}}}\frac{1}{\tau}\bigg(-\frac{\lambda}{16}\frac{e^2E_y^2}{\hbar}\tau^2\gamma_\beta\bigg)\bigg[\bigg(\frac{1}{8}\bigg)\frac{\partial}{\partial k}B_{\boldsymbol{k}} + \bigg(\frac{1}{4}\bigg)\frac{1}{k}B_{\boldsymbol{k}}\bigg]\big[i\xi_k\big(1-\xi_k^2\big)^{1/2}\sin(\theta_{\boldsymbol{k}})\big] \\
& - \frac{\hbar}{4\varepsilon_{\boldsymbol{k}}}\frac{1}{\tau}\bigg(-\frac{\lambda}{16}\frac{e^2E_y^2}{\hbar}\tau^2\gamma_\beta\bigg)\bigg[\bigg(\frac{1}{8}\bigg)\frac{\partial}{\partial k}C_{\boldsymbol{k}} + \bigg(\frac{1}{4}\bigg)\frac{1}{k}C_{\boldsymbol{k}}\bigg]\big[i\xi_k\big(1-\xi_k^2\big)^{1/2}\sin(\theta_{\boldsymbol{k}})\big] \\
& - \frac{\hbar}{4\varepsilon_{\boldsymbol{k}}}\frac{1}{\tau}\bigg(-\frac{\lambda}{16}\frac{e^2E_y^2}{\hbar}\tau^2\gamma_\beta\bigg)\bigg[\bigg(\frac{1}{4}\bigg)\frac{\partial}{\partial k}A_{\boldsymbol{k}} + \bigg(\frac{1}{2}\bigg)\frac{1}{k}A_{\boldsymbol{k}}\bigg]\big[\big(1-\xi_k^2\big)^{1/2}\cos(\theta_{\boldsymbol{k}})\big] \\
& - \frac{\hbar}{4\varepsilon_{\boldsymbol{k}}}\frac{1}{\tau}\bigg(-\frac{\lambda}{16}\frac{e^2E_y^2}{\hbar}\tau^2\gamma_\beta\bigg)\bigg[\bigg(\frac{1}{8}\bigg)\frac{\partial}{\partial k}B_{\boldsymbol{k}} + \bigg(\frac{1}{4}\bigg)\frac{1}{k}B_{\boldsymbol{k}}\bigg]\big[\big(1-\xi_k^2\big)^{1/2}\cos(\theta_{\boldsymbol{k}})\big] \\
& - \frac{\hbar}{4\varepsilon_{\boldsymbol{k}}}\frac{1}{\tau}\bigg(-\frac{\lambda}{16}\frac{e^2E_y^2}{\hbar}\tau^2\gamma_\beta\bigg)\bigg[\bigg(\frac{1}{8}\bigg)\frac{\partial}{\partial k}C_{\boldsymbol{k}} + \bigg(\frac{1}{4}\bigg)\frac{1}{k}C_{\boldsymbol{k}}\bigg]\big[\big(1-\xi_k^2\big)^{1/2}\cos(\theta_{\boldsymbol{k}})\big].
\end{aligned} \tag{D16}$$

Using the explicit form of the diagonal distribution in the first line we get the off-diagonal distribution.

4. Electric field corrected collision integral: β-independent

In this section we calculate the electric field corrected collision integral to first order in warping parameter. It reads

$$\begin{aligned}
[J_E(n_{\rm FD})]^{mm}_{\boldsymbol{k}} = {} & -\frac{2\pi}{\hbar}eE_i\sum_{\boldsymbol{k}'}\frac{\partial}{\partial\epsilon^m_{\boldsymbol{k}'}}\delta\big(\epsilon^m_{\boldsymbol{k}'} - \epsilon^m_{\boldsymbol{k}}\big)\big[n_{\rm FD}\big(\varepsilon^m_{\boldsymbol{k}'}\big) - n_{\rm FD}\big(\varepsilon^m_{\boldsymbol{k}}\big)\big]\,{\rm Im}\bigg\langle\bigg[\bigg(\frac{\partial}{\partial k'_i} + \frac{\partial}{\partial k_i}\bigg)U^{mm}_{\boldsymbol{k}\boldsymbol{k}'}\bigg]U^{mm}_{\boldsymbol{k}'\boldsymbol{k}}\bigg\rangle \\
& + \frac{2\pi}{\hbar}eE_i\sum_{\boldsymbol{k}'}\frac{\partial}{\partial\epsilon^m_{\boldsymbol{k}'}}\delta\big(\epsilon^m_{\boldsymbol{k}'} - \epsilon^m_{\boldsymbol{k}}\big)\big(\mathcal{R}^{mm}_{\boldsymbol{k},i} - \mathcal{R}^{mm}_{\boldsymbol{k}',i}\big)\big[n_{\rm FD}\big(\varepsilon^m_{\boldsymbol{k}'}\big) - n_{\rm FD}\big(\varepsilon^m_{\boldsymbol{k}}\big)\big]\big\langle U^{mm}_{\boldsymbol{k}\boldsymbol{k}'}U^{mm}_{\boldsymbol{k}'\boldsymbol{k}}\big\rangle.
\end{aligned} \tag{D17}$$

In the relaxation time approximation the distribution reads

$$n^{(0)}_{E\boldsymbol{k}} = -\frac{e}{\hbar}E_yA(k)\cos(\theta_{\boldsymbol{k}})\cos(3\theta_{\boldsymbol{k}}) \tag{D18}$$

with coefficient

$$A(k) = \bigg[\frac{1}{4}\bigg(\lambda\frac{\varepsilon_k\xi_{0\boldsymbol{k}}}{\hbar v_F^2}\bigg)\big(1-\xi_k^2\big)\big(-6\xi_k + 6\xi_k^3\big)\bigg]\delta(\varepsilon_{\boldsymbol{k}} - \varepsilon_F). \tag{D19}$$

5. β-independent nonlinear diagonal distribution $n^{(-1)}_{E2}$

With the knowledge of $n^{(0)}_E$, the nonlinear distribution $n^{(-1)}_{E2}$ follows from the equation

$$\big[J_0\big(n^{(-1)}_{E2}\big)\big]^{mm}_{\boldsymbol{k}} = \frac{e\boldsymbol{E}}{\hbar}\cdot\frac{\partial n^{(0)}_E}{\partial\boldsymbol{k}}. \tag{D20}$$

Then, we get the nonlinear distribution

$$n^{(-1)}_{E2\boldsymbol{k}} = -\tau\bigg(\frac{e}{\hbar}E_y\bigg)^2\sin(\theta_{\boldsymbol{k}})\cos(\theta_{\boldsymbol{k}})\cos(3\theta_{\boldsymbol{k}})\frac{\partial A(k)}{\partial k} - \tau\bigg(\frac{e}{\hbar}E_y\bigg)^2\frac{A(k)}{k}\cos(\theta_{\boldsymbol{k}})[-\sin(\theta_{\boldsymbol{k}})\cos(3\theta_{\boldsymbol{k}}) - 3\cos(\theta_{\boldsymbol{k}})\sin(3\theta_{\boldsymbol{k}})]. \tag{D21}$$

6. β-renormalized nonlinear off-diagonal distribution: Second contribution

With the nonlinear diagonal distribution function $n^{(-1)}_{E2\boldsymbol{k}}$ calculated from the β-independent electric field corrected collision integral we can calculate the off-diagonal distribution

$$S^{(0)mm'}_{E2\boldsymbol{k},\beta} = -\frac{\hbar}{i\left(\epsilon^m_{\boldsymbol{k}} - \epsilon^{m'}_{\boldsymbol{k}}\right)}\left[J_\beta\left(n^{(-1)}_{E2}\right)\right]^{mm'}_{\boldsymbol{k}}. \tag{D22}$$

In particular we will calculate the elements

$$S^{(0)+-}_{E2\boldsymbol{k},\beta} = -\frac{\hbar}{i(\epsilon^+_{\boldsymbol{k}} - \epsilon^-_{\boldsymbol{k}})}\left[J_\beta\left(n^{(-1)}_{E2}\right)\right]^{+-}_{\boldsymbol{k}}. \tag{D23}$$

The off-diagonal elements of the collision integral read

$$\begin{aligned}\left[J\left(n^{(-1)}_{E2}\right)\right]^{+-}_{\boldsymbol{k}} &= \frac{\pi}{\hbar}\sum_{\boldsymbol{k}'}\langle U^{++}_{\boldsymbol{k},\boldsymbol{k}'}U^{+-}_{\boldsymbol{k}',\boldsymbol{k}}\rangle_\beta\left(n^{(-1)++}_{E2\boldsymbol{k}} - n^{(-1)++}_{E2\boldsymbol{k}'}\right)\delta(\epsilon^+_{\boldsymbol{k}'} - \epsilon^+_{\boldsymbol{k}}) \\ &= \frac{\pi}{\hbar}\left(n^{(-1)++}_{E2\boldsymbol{k}}\right)\sum_{\boldsymbol{k}'}\langle U^{++}_{\boldsymbol{k},\boldsymbol{k}'}U^{+-}_{\boldsymbol{k}',\boldsymbol{k}}\rangle_\beta\delta(\epsilon^+_{\boldsymbol{k}'} - \epsilon^+_{\boldsymbol{k}}) + \frac{\pi}{\hbar}\sum_{\boldsymbol{k}'}\langle U^{++}_{\boldsymbol{k},\boldsymbol{k}'}U^{+-}_{\boldsymbol{k}',\boldsymbol{k}}\rangle_\beta\left(-n^{(-1)++}_{E2\boldsymbol{k}'}\right)\delta(\epsilon^+_{\boldsymbol{k}'} - \epsilon^+_{\boldsymbol{k}})\end{aligned} \tag{D24}$$

$$\begin{aligned}S^{(0)+-}_{E2\boldsymbol{k},\beta} = &\frac{\hbar}{2\epsilon^+_{\boldsymbol{k}}}\gamma_\beta\left(n^{(-1)++}_{E2\boldsymbol{k}}\right)\left[\frac{i}{4}\right]\left[\xi_k\left(1-\xi_k^2\right)^{1/2}\right] + \frac{\hbar}{2\epsilon^+_{\boldsymbol{k}}}\gamma_\beta\frac{1}{64}\left[\tau\left(\frac{e}{\hbar}E_y\right)^2\frac{\partial A(k)}{\partial k}\right] \\ &\times\left[-\left(1-\xi_k^2\right)^{1/2}3\cos(\theta_{\boldsymbol{k}}) - i\xi_k\left(1-\xi_k^2\right)^{1/2}\sin(\theta_{\boldsymbol{k}})\right] + \frac{\hbar}{2\epsilon^+_{\boldsymbol{k}}}\gamma_\beta\frac{3}{8}\left[\tau\left(\frac{e}{\hbar}E_y\right)^2\frac{A(k)}{k}\right] \\ &\times\left[-\left(1-\xi_k^2\right)^{1/2}\cos(\theta_{\boldsymbol{k}})\sin^2(\theta_{\boldsymbol{k}}) + i\xi_k\left(1-\xi_k^2\right)^{1/2}\sin(\theta_{\boldsymbol{k}})\cos^2(\theta_{\boldsymbol{k}})\right] + \frac{\hbar}{2\epsilon^+_{\boldsymbol{k}}}\gamma_\beta\frac{1}{8}\left[\tau\left(\frac{e}{\hbar}E_y\right)^2\frac{A(k)}{k}\right] \\ &\times\left[-i\xi_k\left(1-\xi_k^2\right)^{1/2}\sin(\theta_{\boldsymbol{k}})\right].\end{aligned} \tag{D25}$$

Using the explicit distribution $n^{(-1)}_{E2\boldsymbol{k}}$ we calculate the off-diagonal distribution.

APPENDIX E: SUBLEADING RESPONSE: β-RENORMALIZED SKEW SCATTERING

In this section we calculate the β-renormalized skew-scattering contribution. To this end, we need to solve the kinetic equation

$$\left[J_0\left(n^{(0)}_{E2,\beta}\right)\right]^{mm}_{\boldsymbol{k}} = -\left[J_0\left(S^{(0)}_{E2,\beta}\right)\right]^{mm}_{\boldsymbol{k}}. \tag{E1}$$

A general expression for the diagonal collision integral as a function of the off-diagonal distribution reads

$$\left[J\left(S^{(0)}_{E2}\right)\right]^{mm}_{\boldsymbol{k}} = \frac{2\pi}{\hbar}\Re\left[\sum_{\boldsymbol{k}'}S^{(0)mm'}_{E2\boldsymbol{k}}\left\langle U^{m'm}_{\boldsymbol{k},\boldsymbol{k}'}U^{mm}_{\boldsymbol{k}',\boldsymbol{k}}\right\rangle\delta\left(\epsilon^m_{\boldsymbol{k}'} - \epsilon^m_{\boldsymbol{k}}\right)\right] - \frac{2\pi}{\hbar}\Re\left[\sum_{\boldsymbol{k}}\left\langle U^{mm'}_{\boldsymbol{k},\boldsymbol{k}'}S^{(0)m'm}_{E2\boldsymbol{k}'}U^{mm}_{\boldsymbol{k}',\boldsymbol{k}}\right\rangle\delta\left(\epsilon^m_{\boldsymbol{k}'} - \epsilon^m_{\boldsymbol{k}}\right)\right]. \tag{E2}$$

This equation is the one used to generate the β-dependent driving terms. So far we have calculated two β-dependent nonlinear off-diagonal distribution. Then we need to use them both to generate two skew-scattering-like contributions, namely, we will solve the kinetic equation

$$\left[J_0\left(n^{(0)}_{E2,\beta(1)}\right)\right]^{mm}_{\boldsymbol{k}} = -\left[J_0\left(S^{(0)}_{E2,\beta(1)}\right)\right]^{mm}_{\boldsymbol{k}}, \tag{E3}$$

where $S^{(0)mm'}_{E2,\beta(1)}$ is the result of a diagonal linear response due to the electric field corrected collision integral with extrinsic spin-orbit scattering potential. We will also solve the kinetic equation

$$\left[J_0\left(n^{(0)}_{E2,\beta(2)}\right)\right]^{mm}_{\boldsymbol{k}} = -\left[J_0\left(S^{(0)}_{E2,\beta(2)}\right)\right]^{mm}_{\boldsymbol{k}}, \tag{E4}$$

where $S^{(0)mm'}_{E2,\beta(2)}$ is the result of a diagonal linear response due to the electric field corrected collision integral without extrinsic spin-orbit scattering potential.

A third contribution arises by solving the equation

$$\left[J_0\left(n^{(0)}_{E2,\beta(3)}\right)\right]^{mm}_{\boldsymbol{k}} = -\left[J_\beta\left(S^{(0)}_{E2}\right)\right]^{mm}_{\boldsymbol{k}}, \tag{E5}$$

where we need a β-independent off-diagonal distribution. However, we find that the first and third contributions cancel each other out.

1. Skew scattering: First contribution

Let us start by calculating the skew-scattering distribution by using the off-diagonal distribution Eq. (D13). We remind that this off-diagonal distribution was found as follows: first we solved the kinetic equation $[J_0(n^{(0)}_{E\boldsymbol{k},\beta})]^{mm}_{\boldsymbol{k}} = -[J_{E,\beta}(n^{(0)}_{\rm FD})]^{mm}_{\boldsymbol{k}}$. This allows us to calculate a linear response distribution $n^{(0)}_{E\boldsymbol{k},\beta}$. Then we use the kinetic equation $[J_0(n^{(-1)}_{E2,\beta})]^{mm}_{\boldsymbol{k}} = (e\boldsymbol{E}/\hbar)\cdot\boldsymbol{\nabla}_{\boldsymbol{k}} n^{(0)}_{E,\beta}$, which allows us to calculte the nonlinear diagonal distribution $n^{(-1)}_{E2,\beta}$. Then we can generate the nonlinear off-diagonal distribution

$$S^{(0)mm'}_{E2\boldsymbol{k},\beta} = -\frac{\hbar}{i\left(\epsilon^m_{\boldsymbol{k}} - \epsilon^{m'}_{\boldsymbol{k}}\right)}\left[J_0\left(n^{(-1)}_{E2,\beta}\right)\right]^{mm'}_{\boldsymbol{k}}. \tag{E6}$$

We use the off-diagonal distribution to generate a driving. Then we solve the kinetic equation $[J(n^{(0)}_{E2,\beta})]^{mm}_{\boldsymbol{k}} = -[J(S^{(0)}_{E2,\beta})]^{mm}_{\boldsymbol{k}}$. A general expression for the diagonal collision integral as a function of an off-diagonal distribution reads

$$\left[J\left(S^{(0)}_{E2,\beta}\right)\right]^{++}_{\boldsymbol{k}} = \frac{2\pi}{\hbar}\Re\left[\sum_{\boldsymbol{k}'} S^{(0)+-}_{E2\boldsymbol{k},\beta}\langle U^{-+}_{\boldsymbol{k},\boldsymbol{k}'}U^{++}_{\boldsymbol{k}',\boldsymbol{k}}\rangle\delta(\epsilon^+_{\boldsymbol{k}'} - \epsilon^+_{\boldsymbol{k}})\right] - \frac{2\pi}{\hbar}\Re\left[\sum_{\boldsymbol{k}}\langle U^{+-}_{\boldsymbol{k},\boldsymbol{k}'}U^{++}_{\boldsymbol{k}',\boldsymbol{k}}\rangle S^{(0)-+}_{E2\boldsymbol{k}',\beta}\delta(\epsilon^+_{\boldsymbol{k}'} - \epsilon^+_{\boldsymbol{k}})\right]. \tag{E7}$$

Then the skew-scattering distribution reads

$$\begin{aligned} n^{(0)++}_{E2,\beta(sk)} = {} & \frac{3\hbar}{4\varepsilon_{\boldsymbol{k}}}\left(-\frac{\lambda}{16}\frac{e^2E_y^2}{\hbar}\tau\gamma_\beta\right)\left[\left(\frac{1}{4}\right)\frac{\partial}{\partial k}A_{\boldsymbol{k}} + \left(\frac{1}{2}\right)\frac{1}{k}A_{\boldsymbol{k}}\right]\left[\xi_k\left(1-\xi_k^2\right)\right][\cos(\theta_{\boldsymbol{k}})] \\ & + \frac{3\hbar}{4\varepsilon_{\boldsymbol{k}}}\left(-\frac{\lambda}{16}\frac{e^2E_y^2}{\hbar}\tau\gamma_\beta\right)\left[\left(\frac{1}{8}\right)\frac{\partial}{\partial k}B_{\boldsymbol{k}} + \left(\frac{1}{4}\right)\frac{1}{k}B_{\boldsymbol{k}}\right]\left[\xi_k\left(1-\xi_k^2\right)\right][\cos(\theta_{\boldsymbol{k}})] \\ & + \frac{3\hbar}{4\varepsilon_{\boldsymbol{k}}}\left(-\frac{\lambda}{16}\frac{e^2E_y^2}{\hbar}\tau\gamma_\beta\right)\left[\left(\frac{1}{8}\right)\frac{\partial}{\partial k}C_{\boldsymbol{k}} + \left(\frac{1}{4}\right)\frac{1}{k}C_{\boldsymbol{k}}\right]\left[\xi_k\left(1-\xi_k^2\right)\right][\cos(\theta_{\boldsymbol{k}})]. \end{aligned} \tag{E8}$$

The current follows from tracing the velocity $v_x = -ev_F(1-\xi_k^2)^{1/2}\cos(\theta_{\boldsymbol{k}})$. We find the response

$$\left[\chi^{(0)}_{xyy}\right]_{sk(1)} = -\lambda\tau\gamma_\beta\frac{\rho(\varepsilon_F)}{\varepsilon_F}\left(\frac{e^3}{\hbar}\right)\xi_F^3\left(1-\xi_k^2\right)\frac{3}{512}\left\{\left(1-\xi_k^2\right)\left[12-48\xi_F^2+40\xi_F^4\right] + \left(1-\xi_F^2\right)^{3/2}\left[-30+89\xi_F^2-90\xi_F^4\right]\right\}. \tag{E9}$$

2. Skew scattering: Second contribution from the β-renormalized off-diagonal distribution

In this section we calculate the skew-scattering distribution due to a β-renormalized off-diagonal distribution coming from β-independent electric field corrected collision integral, namely, we will use the off-diagonal nonlinear distribution

$$\begin{aligned} S^{(0)+-}_{E2\boldsymbol{k},\beta} = {} & \frac{\hbar}{2\epsilon^+_{\boldsymbol{k}}}\gamma_\beta\left(-\tau\left(\frac{e}{\hbar}E_y\right)^2\frac{\partial A(k)}{\partial k}\sin(\theta_{\boldsymbol{k}})\cos(\theta_{\boldsymbol{k}})\cos(3\theta_{\boldsymbol{k}})\right)\left[\frac{i}{4}\right]\left[\xi_k\left(1-\xi_k^2\right)^{1/2}\right] \\ & + \frac{\hbar}{2\epsilon^+_{\boldsymbol{k}}}\gamma_\beta\left(-\tau\left(\frac{e}{\hbar}E_y\right)^2\frac{A(k)}{k}\cos(\theta_{\boldsymbol{k}})[-\sin(\theta_{\boldsymbol{k}})\cos(3\theta_{\boldsymbol{k}}) - 3\cos(\theta_{\boldsymbol{k}})\sin(3\theta_{\boldsymbol{k}})]\right)\left[\frac{i}{4}\right]\left[\xi_k\left(1-\xi_k^2\right)^{1/2}\right] \\ & + \frac{\hbar}{2\epsilon^+_{\boldsymbol{k}}}\gamma_\beta\frac{1}{64}\left[\tau\left(\frac{e}{\hbar}E_y\right)^2\frac{\partial A(k)}{\partial k}\right]\left[-\left(1-\xi_k^2\right)^{1/2}3\cos(\theta_{\boldsymbol{k}}) - i\xi_k\left(1-\xi_k^2\right)^{1/2}\sin(\theta_{\boldsymbol{k}})\right] \\ & + \frac{\hbar}{2\epsilon^+_{\boldsymbol{k}}}\gamma_\beta\frac{3}{8}\left[\tau\left(\frac{e}{\hbar}E_y\right)^2\frac{A(k)}{k}\right]\left[-\left(1-\xi_k^2\right)^{1/2}\cos(\theta_{\boldsymbol{k}})\sin^2(\theta_{\boldsymbol{k}}) + i\xi_k\left(1-\xi_k^2\right)^{1/2}\sin(\theta_{\boldsymbol{k}})\cos^2(\theta_{\boldsymbol{k}})\right] \\ & + \frac{\hbar}{2\epsilon^+_{\boldsymbol{k}}}\gamma_\beta\frac{1}{8}\left[\tau\left(\frac{e}{\hbar}E_y\right)^2\frac{A(k)}{k}\right]\left[-i\xi_k\left(1-\xi_k^2\right)^{1/2}\sin(\theta_{\boldsymbol{k}})\right]. \end{aligned} \tag{E10}$$

Once the driving term is calculated, the distribution follows straightforwardly. It reads

$$\begin{aligned} n^{(0)++}_{E2,\beta,sk} = {} & -\left(\frac{\hbar}{2\epsilon^+_{\boldsymbol{k}}}\gamma_\beta\right)\left[\xi_k\left(1-\xi_k^2\right)\right]\left[\tau\left(\frac{e}{\hbar}E_y\right)^2\frac{\partial A(k)}{\partial k}\right]\left[-\frac{3}{64}\cos(\theta_{\boldsymbol{k}})\right] \\ & - \left(\frac{\hbar}{2\epsilon^+_{\boldsymbol{k}}}\gamma_\beta\right)\left[\xi_k\left(1-\xi_k^2\right)\right]\left[\tau\left(\frac{e}{\hbar}E_y\right)^2\frac{A(k)}{k}\right]\left[-\frac{3}{8}\cos(\theta_{\boldsymbol{k}})\sin^2(\theta_{\boldsymbol{k}})\right] \\ & - \left(\frac{\hbar}{2\epsilon^+_{\boldsymbol{k}}}\gamma_\beta\right)\left[\xi_k\left(1-\xi_k^2\right)\right]\left[\tau\left(\frac{e}{\hbar}E_y\right)^2\frac{\partial A(k)}{\partial k}\right]\left[\frac{1}{32}\cos(\theta_{\boldsymbol{k}})\right] \\ & - \left(\frac{\hbar}{2\epsilon^+_{\boldsymbol{k}}}\gamma_\beta\right)\left[\xi_k\left(1-\xi_k^2\right)\right]\left[\tau\left(\frac{e}{\hbar}E_y\right)^2\frac{A(k)}{k}\right]\left[\frac{1}{16}\cos(\theta_{\boldsymbol{k}})\right] \end{aligned}$$

$$- \left(\frac{\hbar}{2\epsilon_{\boldsymbol{k}}^{+}}\gamma_\beta\right)\left[\xi_k\left(1-\xi_k^2\right)\right]\left[\tau\left(\frac{e}{\hbar}E_y\right)^2\frac{\partial A(k)}{\partial k}\right]\left[-\frac{1}{32}\cos(\theta_{\boldsymbol{k}})\right]$$
$$- \left(\frac{\hbar}{2\epsilon_{\boldsymbol{k}}^{+}}\gamma_\beta\right)\left[\xi_k\left(1-\xi_k^2\right)\right]\left[\tau\left(\frac{e}{\hbar}E_y\right)^2\frac{A(k)}{k}\right]\left[-\frac{1}{16}\cos(\theta_{\boldsymbol{k}})\right]. \tag{E11}$$

The coefficient is

$$\left[\chi^{(0)}_{xyy}\right]_{sk(2)} = -ev_F\frac{\hbar}{2\epsilon_F}\rho(\varepsilon_F)\gamma_\beta\left[\tau\left(\frac{e}{\hbar}\right)^2\right]\left[\frac{3}{256}\left(\lambda\frac{\varepsilon_F\xi_F}{\hbar v_F^2}\right)\xi_F\left(1-\xi_F^2\right)^3\right]\hbar v_F\frac{\xi_F}{\varepsilon_F}\left[-9+12\xi_F^2\right]. \tag{E12}$$

3. Skew scattering: Third contribution

In this section we calculate the contribution related to the driving term

$$\left[J_\beta\left(S^{(0)}_{E2}\right)\right]^{mm}_{\boldsymbol{k}} = \frac{2\pi}{\hbar}\Re\left[\sum_{\boldsymbol{k}'}S^{(0)mm'}_{E2\boldsymbol{k}}\left\langle U^{m'm}_{\boldsymbol{k},\boldsymbol{k}'}U^{mm}_{\boldsymbol{k}',\boldsymbol{k}}\right\rangle_\beta\delta\left(\epsilon^m_{\boldsymbol{k}'}-\epsilon^m_{\boldsymbol{k}}\right)\right] - \frac{2\pi}{\hbar}\Re\left[\sum_{\boldsymbol{k}}\left\langle U^{mm'}_{\boldsymbol{k},\boldsymbol{k}'}S^{(0)m'm}_{E2\boldsymbol{k}'}U^{mm}_{\boldsymbol{k}',\boldsymbol{k}}\right\rangle_\beta\delta\left(\epsilon^m_{\boldsymbol{k}'}-\epsilon^m_{\boldsymbol{k}}\right)\right]. \tag{E13}$$

We should note that it requires a β-independent off-diagonal response. Explicitly

$$\left[J_\beta\left(S^{(0)}_{E2}\right)\right]^{++}_{\boldsymbol{k}} = \frac{2\pi}{\hbar}\Re\left[\sum_{\boldsymbol{k}'}S^{(0)+-}_{E2\boldsymbol{k}}\langle U^{-+}_{\boldsymbol{k},\boldsymbol{k}'}U^{++}_{\boldsymbol{k}',\boldsymbol{k}}\rangle_\beta\delta(\epsilon^+_{\boldsymbol{k}'}-\epsilon^+_{\boldsymbol{k}})\right] - \frac{2\pi}{\hbar}\Re\left[\sum_{\boldsymbol{k}}\langle U^{+-}_{\boldsymbol{k},\boldsymbol{k}'}U^{++}_{\boldsymbol{k}',\boldsymbol{k}}\rangle_\beta S^{(0)-+}_{E2\boldsymbol{k}'}\delta(\epsilon^+_{\boldsymbol{k}'}-\epsilon^+_{\boldsymbol{k}})\right]. \tag{E14}$$

Given the driving term, the distribution function follows easily. It reads

$$n^{(0)++}_{sk,E^2\beta} = \tau\gamma_\beta\left[\frac{\hbar}{\epsilon_{\boldsymbol{k}}}\left[\xi_k\left(1-\xi_k^2\right)\right]\right]\left[-\left(\frac{e}{\hbar}E_y\right)^2\frac{\partial A(k)}{\partial k}\right]\left[\frac{3}{128}\cos(\theta_{\boldsymbol{k}})\right] \tag{E15}$$
$$+\tau\gamma_\beta\left[\frac{\hbar}{\epsilon_{\boldsymbol{k}}}\left[\xi_k\left(1-\xi_k^2\right)\right]\right]\left[-\left(\frac{e}{\hbar}E_y\right)^2\frac{A(k)}{k}\right]\left[\frac{3}{16}\cos(\theta_{\boldsymbol{k}})\sin^2(\theta_{\boldsymbol{k}})\right] \tag{E16}$$

with the coefficient,

$$A(k) = \left[\frac{1}{4}\left(\lambda\frac{\varepsilon_{\boldsymbol{k}}\xi_{0\boldsymbol{k}}}{\hbar v_F^2}\right)\left(1-\xi_k^2\right)\left(-6\xi_k+6\xi_k^3\right)\right][\delta(\varepsilon_{\boldsymbol{k}}-\varepsilon_F)]. \tag{E17}$$

The response reads

$$\left[\chi^{(0)}_{xyy}\right]_{sk(3)} = \lambda\tau\gamma_\beta\frac{\rho(\varepsilon_F)}{\varepsilon_F}\left(\frac{e^3}{\hbar}\right)\xi_F^3\left(1-\xi_k^2\right)\frac{3}{512}\left\{\left(1-\xi_k^2\right)\left[12-48\xi_F^2+40\xi_F^4\right]+\left(1-\xi_F^2\right)^{3/2}\left[-30+89\xi_F^2-90\xi_F^4\right]\right\}. \tag{E18}$$

APPENDIX F: ELECTRON PHONON SCATTERING

In this section we study the temperature dependence of the nonlinear conductivity. To this end we consider electron-phonon interaction through phonon scattering effect. The effect comes from the collision integral [60] in Eq. (9).

1. High-temperature regime of the momentum relaxation time

In the high-temperature regime the phonon occupation can be approximated as $N_{\boldsymbol{q}} \approx k_BT/\hbar\omega_q$. Also, we can take $(N_{\boldsymbol{q}}+1) \approx N_{\boldsymbol{q}}$. The collision integral Eq. (9) then reads

$$[J_{\rm ep}(f)]^{++}_{\boldsymbol{k}} \approx -f^+_{\boldsymbol{k}}\frac{2\pi}{\hbar}\sum_{\boldsymbol{k}'}\sum_{\boldsymbol{q}}|D_{\boldsymbol{q}}|^2\delta(\hbar\omega_{\boldsymbol{q}}+\varepsilon^+_{\boldsymbol{k}'}-\varepsilon^+_{\boldsymbol{k}})\left(\frac{k_BT}{\hbar\omega_q}\right)\left[\frac{f^+_{\boldsymbol{k}'}}{f^+_{\boldsymbol{k}}}-1\right]\delta_{\boldsymbol{k}',\boldsymbol{k}-\boldsymbol{q}} - f^+_{\boldsymbol{k}}\frac{2\pi}{\hbar}\sum_{\boldsymbol{k}''}\sum_{\boldsymbol{q}}|D_{\boldsymbol{q}}|^2$$
$$\times\,\delta(\hbar\omega_{\boldsymbol{q}}+\varepsilon^+_{\boldsymbol{k}}-\varepsilon^+_{\boldsymbol{k}''})\left(\frac{k_BT}{\hbar\omega_q}\right)\left[\frac{f^+_{\boldsymbol{k}''}}{f^+_{\boldsymbol{k}}}-1\right]\delta_{\boldsymbol{k}'',\boldsymbol{k}+\boldsymbol{q}}. \tag{F1}$$

In the constant relaxation time approximation we take $[J_{\rm ep}(f)]^{++}_{\boldsymbol{k}} = f_{\boldsymbol{k}}/\tau_{\rm ep}$. Then the relaxation time is defined as

$$\frac{1}{\tau_{\rm ep}} \approx \frac{2\pi}{\hbar}\sum_{\boldsymbol{q}}|D_{\boldsymbol{q}}|^2\delta(\hbar\omega_{\boldsymbol{q}}+\varepsilon^+_{\boldsymbol{k}-\boldsymbol{q}}-\varepsilon^+_{\boldsymbol{k}})\left(\frac{k_BT}{\hbar\omega_q}\right)[1-\cos(\theta_{\boldsymbol{k},\boldsymbol{k}-\boldsymbol{q}})]$$
$$+\frac{2\pi}{\hbar}\sum_{\boldsymbol{q}}|D_{\boldsymbol{q}}|^2\delta(\hbar\omega_{\boldsymbol{q}}+\varepsilon^+_{\boldsymbol{k}}-\varepsilon^+_{\boldsymbol{k}+\boldsymbol{q}})\left(\frac{k_BT}{\hbar\omega_q}\right)[1-\cos(\theta_{\boldsymbol{k},\boldsymbol{k}+\boldsymbol{q}})]. \tag{F2}$$

About $\boldsymbol{k}=0$ the relation dispersion can be approximated to a normal metal one. In this case the delta functions can be written as

$$\delta(\hbar\omega_{\boldsymbol{q}}+\varepsilon^{+}_{\boldsymbol{k}-\boldsymbol{q}}-\varepsilon^{+}_{\boldsymbol{k}})\approx\delta[\hbar\omega_{\boldsymbol{q}}+\eta\hbar^2q^2-2\eta\hbar^2k_Fq\cos(\theta)]=\left(\frac{1}{\hbar^2\eta 2k_Fq}\right)\delta[b_+-\cos(\theta)] \tag{F3}$$

$$\delta(\hbar\omega_{\boldsymbol{q}}+\varepsilon^{+}_{\boldsymbol{k}}-\varepsilon^{+}_{\boldsymbol{k}+\boldsymbol{q}})\approx\delta[\hbar\omega_{\boldsymbol{q}}-\eta\hbar^2q^2-2\eta\hbar^2k_Fq\cos(\theta)]=\left(\frac{1}{\hbar^2\eta 2k_Fq}\right)\delta[b_--\cos(\theta)], \tag{F4}$$

where $b_\pm=\frac{\hbar\omega_q\pm\eta\hbar^2q^2}{\hbar^2\eta 2k_Fq}$. The integral is then written as

$$\begin{aligned}\frac{1}{\tau_{\rm ep}}\approx{}&\frac{2\pi}{\hbar}\left(\frac{1}{2\pi}\right)\int qdq\left(\frac{k_BT}{\hbar\omega_q}\right)\left(\frac{1}{\hbar^2\eta 2k_Fq}\right)|D_{\boldsymbol{q}}|^2\left(\frac{1}{2\pi}\right)\int d\theta\delta[b_+-\cos(\theta)][1-\cos(\theta_{\boldsymbol{k},\boldsymbol{k}-\boldsymbol{q}})]\\&+\frac{2\pi}{\hbar}\left(\frac{1}{2\pi}\right)\int qdq\left(\frac{k_BT}{\hbar\omega_q}\right)\left(\frac{1}{\hbar^2\eta 2k_Fq}\right)|D_{\boldsymbol{q}}|^2\left(\frac{1}{2\pi}\right)\int d\theta\delta[b_--\cos(\theta)][1-\cos(\theta_{\boldsymbol{k},\boldsymbol{k}+\boldsymbol{q}})].\end{aligned} \tag{F5}$$

The delta function is written as

$$\delta[b_\pm-\cos(\theta)]=\delta(\theta-\theta_i)/|\sin(\theta_i)|, \tag{F6}$$

where $\theta_i=\arccos(b_\pm)$ and then $\sin(\theta_i)=\sqrt{1-b_\pm^2}$. After performing the angular integral we get

$$\begin{aligned}\frac{1}{\tau_{\rm ep}}\approx{}&\frac{2\pi}{\hbar}\left(\frac{1}{2\pi}\right)\left(\frac{1}{\hbar^2\eta 2k_F}\right)\left(\frac{1}{2\pi}\right)\int dq\left(\frac{k_BT}{\hbar\omega_q}\right)|D_{\boldsymbol{q}}|^2\frac{1}{\sqrt{1-b_+^2}}(1-b_+)\\&+\frac{2\pi}{\hbar}\left(\frac{1}{2\pi}\right)\left(\frac{1}{\hbar^2\eta 2k_F}\right)\left(\frac{1}{2\pi}\right)\int dq\left(\frac{k_BT}{\hbar\omega_q}\right)|D_{\boldsymbol{q}}|^2\frac{1}{\sqrt{1-b_-^2}}(1-b_-).\end{aligned} \tag{F7}$$

For quasielastic process we neglect the phonon energy $\hbar\omega_q$ and then $b_\pm\to\pm q/2k_F$. This is equivalent to neglect the phonon energy in the delta functions. Then we get

$$\begin{aligned}\frac{1}{\tau_{\rm ep}}\approx{}&\frac{2\pi}{\hbar}\left(\frac{1}{2\pi}\right)\left(\frac{1}{\hbar^2\eta 2k_F}\right)\left(\frac{1}{2\pi}\right)\int dq\left(\frac{k_BT}{\hbar\omega_q}\right)|D_{\boldsymbol{q}}|^2\frac{1}{\sqrt{1-(q/2k_F)^2}}(1-q/2k_F)\\&+\frac{2\pi}{\hbar}\left(\frac{1}{2\pi}\right)\left(\frac{1}{\hbar^2\eta 2k_F}\right)\left(\frac{1}{2\pi}\right)\int dq\left(\frac{k_BT}{\hbar\omega_q}\right)|D_{\boldsymbol{q}}|^2\frac{1}{\sqrt{1-(q/2k_F)^2}}(1+q/2k_F).\end{aligned} \tag{F8}$$

We now use the matrix elements calculated in Ref. [58], namely

$$D_{\boldsymbol{q}}=\alpha\sqrt{\frac{C}{qA}}\left(\frac{\omega_q^{(0)}}{c_l}\right)^2\sqrt{\frac{\hbar}{2\rho_M\omega_q^{(0)}}}\Lambda_l(q), \tag{F9}$$

with $\Lambda(q)\approx 1$. The integral over momentum is then written as

$$\frac{1}{\tau_{\rm ep}}\approx 2\frac{2\pi}{\hbar}\left(\frac{1}{2\pi}\right)\left(\frac{1}{\hbar^2\eta 2k_F}\right)\left(\frac{1}{2\pi}\right)\left(\frac{k_BT}{\hbar}\right)\alpha^2\left(\frac{C}{A}\right)\left(\frac{c_R}{c_l}\right)^4\left(\frac{\hbar}{2\rho_Mc_R^2}\right)\int dq\frac{q}{\sqrt{1-(q/2k_F)^2}}, \tag{F10}$$

where we used $\omega_q=c_Rq$. The last integral is calculated analytically to be

$$\frac{1}{\tau_{\rm ep}}\approx 2\frac{2\pi}{\hbar}\left(\frac{1}{2\pi}\right)\left(\frac{1}{\hbar^2\eta 2k_F}\right)\left(\frac{1}{2\pi}\right)\left(\frac{k_BT}{\hbar}\right)\alpha^2\left(\frac{C}{A}\right)\left(\frac{c_R}{c_l}\right)^4\left(\frac{\hbar}{2\rho_Mc_R^2}\right)[-(2k_F)^2\sqrt{1-(q/2k_F)^2}]|_0^{q_{\rm max}}. \tag{F11}$$

Due to the delta function, the momentum q has a restriction, which is $q_{\rm max}=2k_F$. Then we get the relaxation time

$$\frac{1}{\tau_{\rm ep}}\approx 2\frac{2\pi}{\hbar}\left(\frac{1}{2\pi}\right)\left(\frac{1}{\hbar^2\eta 2k_F}\right)\left(\frac{1}{2\pi}\right)\left(\frac{k_BT}{\hbar}\right)\alpha^2\left(\frac{C}{A}\right)\left(\frac{c_R}{c_l}\right)^4\left(\frac{\hbar}{2\rho_Mc_R^2}\right)(2k_F)^2. \tag{F12}$$

After some cancellations, it can be cast as

$$\frac{1}{\tau_{\rm ep}}\approx\frac{1}{\pi}\left(\frac{k_BT}{\hbar}\right)\left(\frac{C}{A}\right)\left(\frac{c_R}{c_l}\right)^4\left(\frac{1}{2\eta\rho_Mc_R^2}\right)\left(\frac{\alpha^2}{\hbar^2}\right)(2k_F). \tag{F13}$$

We recall that $1/\eta=M/v_F^2$ is an effective mass, where M is the gap. This is in view of the expansion of the relation dispersion about $\boldsymbol{k}=0$.

[1] Z. He and H. Weng, Giant nonlinear Hall effect in twisted bilayer WTe_2, npj Quantum Mater. **6**, 101 (2021).

[2] M. Huang, Z. Wu, J. Hu, X. Cai, E. Li, L. An, X. Feng, Z. Ye, N. Lin, K. T. Law, and N. Wang, Giant nonlinear Hall effect in twisted bilayer WSe_2, Natl. Sci. Rev. **10**, nwac232 (2023).

[3] J. Duan, Y. Jian, Y. Gao, H. Peng, J. Zhong, Q. Feng, J. Mao, and Y. Yao, Giant second-order nonlinear Hall effect in twisted bilayer graphene, Phys. Rev. Lett. **129**, 186801 (2022).

[4] H.-J. Tien, H. Lin, L. Fu, and T.-R. Chang, Quantum metric non-linear Hall effect in an antiferromagnetic topological insulator thin-film $EuSn_2As_2$, Mater. Today Quantum **5**, 100027 (2025).

[5] M. S. Okyay, M. Choi, Q. Xu, A. P. Diéguez, M. Del Ben, K. Z. Ibrahim, and B. M. Wong, Unconventional nonlinear Hall effects in twisted multilayer 2D materials, npj 2D Mater. Appl. **9**, 1 (2025).

[6] D. Kaplan, T. Holder, and B. Yan, Unification of nonlinear anomalous Hall effect and nonreciprocal magnetoresistance in metals by the quantum geometry, Phys. Rev. Lett. **132**, 026301 (2024).

[7] M. T. Mercaldo, M. Cuoco, and C. Ortix, Nonlinear planar magnetotransport as a probe of the topology of surface states, Phys. Rev. B **111**, 155442 (2025).

[8] R. B. Atencia, D. Xiao, and D. Culcer, Disorder in the nonlinear anomalous Hall effect of $\mathcal{PT}$-symmetric Dirac fermions, Phys. Rev. B **108**, L201115 (2023).

[9] I. Sodemann and L. Fu, Quantum nonlinear Hall effect induced by Berry curvature dipole in time-reversal invariant materials, Phys. Rev. Lett. **115**, 216806 (2015).

[10] S. Nandy and I. Sodemann, Symmetry and quantum kinetics of the nonlinear Hall effect, Phys. Rev. B **100**, 195117 (2019).

[11] P. Makushko, S. Kovalev, Y. Zabila, I. Ilyakov, A. Ponomaryov, A. Arshad, G. L. Prajapati, T. V. A. G. de Oliveira, J.-C. Deinert, P. Chekhonin, I. Veremchuk, T. Kosub, Y. Skourski, F. Ganss, D. Makarov, and C. Ortix, A tunable room-temperature nonlinear Hall effect in elemental bismuth thin films, Nature Electron. **7**, 207 (2024).

[12] L. Min, H. Tan, Z. Xie, L. Miao, R. Zhang, S. H. Lee, V. Gopalan, C.-X. Liu, N. Alem, B. Yan, and Z. Mao, Strong room-temperature bulk nonlinear Hall effect in a spin-valley locked Dirac material, Nature Commun. **14**, 364 (2023).

[13] S. Wang, X. Li, H. Zhang, B. Chen, H. Xie, C. Li, F. Fei, S. Zhang, and F. Song, Nonlinear Hall effect and scaling law in Sb-doped topological insulator $MnBi_4Te_7$, Appl. Phys. Lett. **124**, 153102 (2024).

[14] T. Nishijima, T. Watanabe, H. Sekiguchi, Y. Ando, E. Shigematsu, R. Ohshima, S. Kuroda, and M. Shiraishi, Ferroic Berry curvature dipole in a topological crystalline insulator at room temperature, Nano Lett. **23**, 2247 (2023).

[15] J. Han, T. Uchimura, Y. Araki, J.-Y. Yoon, Y. Takeuchi, Y. Yamane, S. Kanai, J. Ieda, H. Ohno, and S. Fukami, Room-temperature flexible manipulation of the quantum-metric structure in a topological chiral antiferromagnet, Nature Phys. **20**, 1110 (2024).

[16] L. Min, Y. Zhang, Z. Xie, S. V. G. Ayyagari, L. Miao, Y. Onishi, S. H. Lee, Y. Wang, N. Alem, L. Fu, and Z. Mao, Colossal room-temperature non-reciprocal Hall effect, Nature Mater. **23**, 1671 (2024).

[17] Y. Zhang and L. Fu, Terahertz detection based on nonlinear Hall effect without magnetic field, Proc. Natl. Acad. Sci. USA **118**, e2100736118 (2021).

[18] C. Guo, Z. Chen, X. Yu, L. Zhang, X. Wang, X. Chen, and L. Wang, Ultrasensitive anisotropic room-temperature terahertz photodetector based on an intrinsic magnetic topological insulator $MnBi_2Te_4$, Nano Lett. **22**, 7492 (2022).

[19] Z. Hu, L. Zhang, A. Chakraborty, G. D'Olimpio, J. Fujii, A. Ge, Y. Zhou, C. Liu, A. Agarwal, I. Vobornik, D. Farias, C.-N. Kuo, C. S. Lue, A. Politano, S.-W. Wang, W. Hu, X. Chen, W. Lu, and L. Wang, Terahertz nonlinear Hall rectifiers based on spin-polarized topological electronic states in 1T-$CoTe_2$, Adv. Mater. **35**, 2209557 (2023).

[20] Y. Li, W. Yu, K. Zhang, N. Cui, T. Yun, X. Xia, Y. Jiang, G. Zhang, H. Mu, and S. Lin, Two-dimensional topological semimetals: An emerging candidate for terahertz detectors and on-chip integration, Mater. Horiz. **11**, 2572 (2024).

[21] E. Mönch, M. D. Moldavskaya, L. E. Golub, V. V. Bel'kov, J. Wunderlich, D. Weiss, J. V. Gumenjuk-Sichevska, C. Niu, P. D. Ye, and S. D. Ganichev, Terahertz radiation driven nonlinear transport phenomena in two-dimensional tellurene, Nano Lett. **25**, 476 (2025).

[22] H. Wang and X. Qian, Electrically and magnetically switchable nonlinear photocurrent in PT-symmetric magnetic topological quantum materials, npj Comput. Mater. **6**, 199 (2020).

[23] Y. Shen, L. Primeau, J. Li, T.-D. Nguyen, D. Mandrus, Y. C. Lin, and Y. Zhang, Nonlinear photocurrent in quantum materials for broadband photodetection, Prog. Quantum Electron. **97**, 100535 (2024).

[24] J. Xiao, Y. Wang, H. Wang, C. D. Pemmaraju, S. Wang, P. Muscher, E. J. Sie, C. M. Nyby, T. P. Devereaux, X. Qian, X. Zhang, and A. M. Lindenberg, Berry curvature memory through electrically driven stacking transitions, Nature Phys. **16**, 1028 (2020).

[25] D. Kumar, C.-H. Hsu, R. Sharma, T.-R. Chang, P. Yu, J. Wang, G. Eda, G. Liang, and H. Yang, Room-temperature nonlinear Hall effect and wireless radiofrequency rectification in Weyl semimetal $TaIrTe_4$, Nature Nanotechnol. **16**, 421 (2021).

[26] B. Cheng, Y. Gao, Z. Zheng, S. Chen, Z. Liu, L. Zhang, Q. Zhu, H. Li, L. Li, and C. Zeng, Giant nonlinear Hall and wireless rectification effects at room temperature in the elemental semiconductor tellurium, Nature Commun. **15**, 5513 (2024).

[27] D. Kumar, R. Sharma, F. Wang, Y. Liu, S. Zhao, and H. Yang, Quantum rectification based on room temperature multidirectional nonlinearity in Bi_2Te_3, Nano Lett. **24**, 12545 (2024).

[28] H. Liu, T. Y. Lim, S. Tian, J. Zhai, D. Xiang, T. Liu, T.-R. Chang, P. He, and J. Shen, Giant nonlinear Hall effect induced ultrahigh rectification in a Weyl semiconductor, Adv. Electron. Mater. **11**, 2400648 (2025).

[29] Z. Z. Du, C. M. Wang, S. Li, H.-Z. Lu, and X. C. Xie, Disorder-induced nonlinear Hall effect with time-reversal symmetry, Nature Commun. **10**, 3047 (2019).

[30] Z. Z. Du, C. M. Wang, H.-P. Sun, H.-Z. Lu, and X. C. Xie, Quantum theory of the nonlinear Hall effect, Nature Commun. **12**, 5038 (2021).

[31] Z. Z. Du, H.-Z. Lu, and X. C. Xie, Nonlinear Hall effects, Nature Rev. Phys. **3**, 744 (2021).

[32] C. Ortix, Nonlinear Hall effect with time-reversal symmetry: Theory and material realizations, Adv. Quantum Technol. **4**, 2100056 (2021).

[33] D. Ma, A. Arora, G. Vignale, and J. C. W. Song, Anomalous skew-scattering nonlinear Hall effect and chiral photocurrents in $\mathcal{PT}$-symmetric antiferromagnets, Phys. Rev. Lett. **131**, 076601 (2023).

[34] B. T. Zhou, C.-P. Zhang, and K. T. Law, Highly tunable nonlinear Hall effects induced by spin-orbit couplings in strained polar transition-metal dichalcogenides, Phys. Rev. Appl. **13**, 024053 (2020).

[35] C.-P. Zhang, J. Xiao, B. T. Zhou, J.-X. Hu, Y.-M. Xie, B. Yan, and K. T. Law, Giant nonlinear Hall effect in strained twisted bilayer graphene, Phys. Rev. B **106**, L041111 (2022).

[36] C.-L. Zhang, T. Liang, Y. Kaneko, N. Nagaosa, and Y. Tokura, Giant Berry curvature dipole density in a ferroelectric Weyl semimetal, npj Quantum Mater. **7**, 103 (2022).

[37] E. J. König, M. Dzero, A. Levchenko, and D. A. Pesin, Gyrotropic Hall effect in Berry-curved materials, Phys. Rev. B **99**, 155404 (2019).

[38] H. Isobe, S.-Y. Xu, and L. Fu, High-frequency rectification via chiral Bloch electrons, Sci. Adv. **6**, eaay2497 (2020).

[39] S. Liu, R. Burgos, E. Zhang, N. Wang, X.-B. Qiang, C. Li, Q. Zhang, Z. Z. Du, R. Zheng, J. Chen, Q.-H. Xu, K. Leng, W. Gao, F. Xiu, D. Culcer, and K. P. Loh, Room-temperature nonlinear transport and microwave rectification in antiferromagnetic $MnBi_2Te_4$ films, Commun. Phys. **7**, 413 (2024).

[40] S. Lai, H. Liu, Z. Zhang, J. Zhao, X. Feng, N. Wang, C. Tang, Y. Liu, K. S. Novoselov, S. A. Yang, and Wei-bo Gao, Third-order nonlinear Hall effect induced by the Berry-connection polarizability tensor, Nature Nanotechnol. **16**, 869 (2021).

[41] C. Wang, R.-C. Xiao, H. Liu, Z. Zhang, S. Lai, C. Zhu, H. Cai, N. Wang, S. Chen, Y. Deng, Z. Liu, S. A. Yang, and W.-B. Gao, Room-temperature third-order nonlinear Hall effect in Weyl semimetal $TaIrTe_4$, Natl. Sci. Rev. **9**, nwac020 (2022).

[42] S. Sankar, R. Liu, C.-P. Zhang, Q.-F. Li, C. Chen, X.-J. Gao, J. Zheng, Y.-H. Lin, K. Qian, R.-P. Yu, X. Zhang, Z. Y. Meng, K. T. Law, Q. Shao, and B. Jäck, Experimental evidence for a Berry curvature quadrupole in an antiferromagnet, Phys. Rev. X **14**, 021046 (2024).

[43] T. Nag, S. K. Das, C. Zeng, and S. Nandy, Third-order Hall effect in the surface states of a topological insulator, Phys. Rev. B **107**, 245141 (2023).

[44] Y. Gao, Z.-Q. Zhang, and K.-H. Ding, Third-order nonlinear Hall effect in two-dimensional Dirac systems, New J. Phys. **25**, 053013 (2023).

[45] P. He, H. Isobe, G. K. W. Koon, J. Y. Tan, J. Hu, J. Li, N. Nagaosa, and J. Shen, Third-order nonlinear Hall effect in a quantum Hall system, Nature Nanotechnol. **19**, 1460 (2024).

[46] X. Zhang, K. Sun, and Z. Y. Meng, Third-order anomalous Hall response to the Fermi-surface topology in magnetic materials, Phys. Rev. B **110**, 165140 (2024).

[47] S. Li, X. Wang, Z. Yang, L. Zhang, S. L. Teo, M. Lin, R. He, N. Wang, P. Song, W. Tian, X. J. Loh, Q. Zhu, B. Sun, and X. R. Wang, Giant third-order nonlinear Hall effect in misfit layer compound $(SnS)_{1.17}(NbS_2)_3$, ACS Appl. Mater. Interfaces **16**, 11043 (2024).

[48] D. Mandal, S. Sarkar, K. Das, and A. Agarwal, Quantum geometry induced third-order nonlinear transport responses, Phys. Rev. B **110**, 195131 (2024).

[49] W.-C. Lee, C. Wu, D. P. Arovas, and S.-C. Zhang, Quasiparticle interference on the surface of the topological insulator bi_2te_3, Phys. Rev. B **80**, 245439 (2009).

[50] P. Adroguer, W. E. Liu, D. Culcer, and E. M. Hankiewicz, Conductivity corrections for topological insulators with spin-orbit impurities: Hikami-Larkin-Nagaoka formula revisited, Phys. Rev. B **92**, 241402(R) (2015).

[51] D. Culcer, A. Sekine, and A. H. MacDonald, Interband coherence response to electric fields in crystals: Berry-phase contributions and disorder effects, Phys. Rev. B **96**, 035106 (2017).

[52] R. B. Atencia, Q. Niu, and D. Culcer, Semiclassical response of disordered conductors: Extrinsic carrier velocity and spin and field-corrected collision integral, Phys. Rev. Res. **4**, 013001 (2022).

[53] M. Mehraeen, Quantum kinetic theory of quadratic responses, Phys. Rev. B **110**, 174423 (2024).

[54] E. H. Hwang and S. Das Sarma, Acoustic phonon scattering limited carrier mobility in two-dimensional extrinsic graphene, Phys. Rev. B **77**, 115449 (2008).

[55] B.-L. Huang and M. Kaviany, Ab initio and molecular dynamics predictions for electron and phonon transport in bismuth telluride, Phys. Rev. B **77**, 125209 (2008).

[56] X. Zhu, L. Santos, R. Sankar, S. Chikara, C. Howard, F. C. Chou, C. Chamon, and M. El-Batanouny, Interaction of phonons and Dirac fermions on the surface of Bi_2Se_3: A strong Kohn anomaly, Phys. Rev. Lett. **107**, 186102 (2011).

[57] K. Kaasbjerg, K. S. Thygesen, and K. W. Jacobsen, Unraveling the acoustic electron-phonon interaction in graphene, Phys. Rev. B **85**, 165440 (2012).

[58] V. Parente, A. Tagliacozzo, F. von Oppen, and F. Guinea, Electron-phonon interaction on the surface of a three-dimensional topological insulator, Phys. Rev. B **88**, 075432 (2013).

[59] S. Giraud and R. Egger, Electron-phonon scattering in topological insulators, Phys. Rev. B **83**, 245322 (2011).

[60] J. Wang and D. Culcer, Suppression of the Kondo resistivity minimum in topological insulators, Phys. Rev. B **88**, 125140 (2013).

[61] L. Fu, Hexagonal warping effects in the surface states of the topological insulator bi_2te_3, Phys. Rev. Lett. **103**, 266801 (2009).

[62] G. Naselli, A. G. Moghaddam, S. Di Napoli, V. Vildosola, I. C. Fulga, J. van den Brink, and J. I. Facio, Magnetic warping in topological insulators, Phys. Rev. Res. **4**, 033198 (2022).

[63] P. He, H. Isobe, D. Zhu, C.-H. Hsu, L. Fu, and H. Yang, Quantum frequency doubling in the topological insulator Bi_2Se_3, Nature Commun. **12**, 698 (2021).

[64] X. F. Lu, C.-P. Zhang, N. Wang, D. Zhao, X. Zhou, W. Gao, X. H. Chen, K. T. Law, and K. P. Loh, Nonlinear transport and radio frequency rectification in BiTeBr at room temperature, Nature Commun. **15**, 245 (2024).

[65] D. Culcer, E. M. Hankiewicz, G. Vignale, and R. Winkler, Side jumps in the spin Hall effect: Construction of the Boltzmann collision integral, Phys. Rev. B **81**, 125332 (2010).

[66] N. A. Sinitsyn, Q. Niu, and A. H. MacDonald, Coordinate shift in the semiclassical Boltzmann equation and the anomalous Hall effect, Phys. Rev. B **73**, 075318 (2006).

[67] N. A. Sinitsyn, A. H. MacDonald, T. Jungwirth, V. K. Dugaev, and J. Sinova, Anomalous Hall effect in a two-dimensional Dirac band: The link between the Kubo-Streda formula and the semiclassical Boltzmann equation approach, Phys. Rev. B **75**, 045315 (2007).

[68] N. A. Sinitsyn, Semiclassical theories of the anomalous Hall effect, J. Phys.: Condens. Matter **20**, 023201 (2008).

[69] Q. Ma, S.-Y. Xu, H. Shen, D. MacNeill, V. Fatemi, T.-R. Chang, A. M. Mier Valdivia, S. Wu, Z. Du, C.-H. Hsu, S. Fang, Q. D. Gibson, K. Watanabe, T. Taniguchi, R. J. Cava, E. Kaxiras, H.-Z. Lu, H. Lin, L. Fu, N. Gedik, *et al.*, Observation of the nonlinear Hall effect under time-reversal-symmetric conditions, Nature (London) **565**, 337 (2019).

[70] S. Sinha, P. C. Adak, A. Chakraborty, K. Das, K. Debnath, L. D. V. Sangani, K. Watanabe, T. Taniguchi, U. V. Waghmare, A. Agarwal, and M. M. Deshmukh, Berry curvature dipole senses topological transition in a moirésuperlattice, Nature Phys. **18**, 765 (2022).

[71] Y. Zhang, J. van den Brink, C. Felser, and B. Yan, Electrically tuneable nonlinear anomalous Hall effect in two-dimensional transition-metal dichalcogenides WTe_2 and $MoTe_2$, 2D Mater. **5**, 044001 (2018).

[72] Z. Z. Du, C. M. Wang, H.-Z. Lu, and X. C. Xie, Band signatures for strong nonlinear Hall effect in bilayer WTe_2, Phys. Rev. Lett. **121**, 266601 (2018).

[73] J. I. Facio, D. Efremov, K. Koepernik, J.-S. You, I. Sodemann, and J. van den Brink, Strongly enhanced Berry dipole at topological phase transitions in BiTeI, Phys. Rev. Lett. **121**, 246403 (2018).

[74] Y. Zhang, Y. Sun, and B. Yan, Berry curvature dipole in Weyl semimetal materials: An ab initio study, Phys. Rev. B **97**, 041101(R) (2018).

[75] C. Wang, Y. Gao, and D. Xiao, Intrinsic nonlinear Hall effect in antiferromagnetic tetragonal CuMnAs, Phys. Rev. Lett. **127**, 277201 (2021).

[76] H. Liu, J. Zhao, Y.-X. Huang, W. Wu, X.-L. Sheng, C. Xiao, and S. A. Yang, Intrinsic second-order anomalous Hall effect and its application in compensated antiferromagnets, Phys. Rev. Lett. **127**, 277202 (2021).

[77] A. Gao, Y.-F. Liu, J.-X. Qiu, B. Ghosh, T. V. Trevisan, Y. Onishi, C. Hu, T. Qian, H.-J. Tien, S.-W. Chen, M. Huang, D. Bérubé, H. Li, C. Tzschaschel, T. Dinh, Z. Sun, S.-C. Ho, S.-W. Lien, B. Singh, K. Watanabe, *et al.*, Quantum metric nonlinear Hall effect in a topological antiferromagnetic heterostructure, Science **381**, 181 (2023).

[78] K. Das, S. Lahiri, R. B. Atencia, D. Culcer, and A. Agarwal, Intrinsic nonlinear conductivities induced by the quantum metric, Phys. Rev. B **108**, L201405 (2023).

[79] N. Wang, D. Kaplan, Z. Zhang, T. Holder, N. Cao, A. Wang, X. Zhou, F. Zhou, Z. Jiang, C. Zhang, S. Ru, H. Cai, K. Watanabe, T. Taniguchi, B. Yan, and W. Gao, Quantum-metric-induced nonlinear transport in a topological antiferromagnet, Nature (London) **621**, 487 (2023).

[80] K. Kang, T. Li, E. Sohn, J. Shan, and K. F. Mak, Nonlinear anomalous Hall effect in few-layer WTe_2, Nature Mater. **18**, 324 (2019).

[81] A. Tiwari, F. Chen, S. Zhong, E. Drueke, J. Koo, A. Kaczmarek, C. Xiao, J. Gao, X. Luo, Q. Niu, Y. Sun, B. Yan, L. Zhao, and A. W. Tsen, Giant c-axis nonlinear anomalous Hall effect in Td-$MoTe_2$ and WTe_2, Nature Commun. **12**, 2049 (2021).

[82] P. He, G. K. W. Koon, H. Isobe, J. Y. Tan, J. Hu, A. H. C. Neto, L. Fu, and H. Yang, Graphene moirésuperlattices with giant quantum nonlinearity of chiral Bloch electrons, Nature Nanotechnol. **17**, 378 (2022).

[83] J. Kötzler and W. Gil, Anomalous Hall resistivity of cobalt films: Evidence for the intrinsic spin-orbit effect, Phys. Rev. B **72**, 060412(R) (2005).

[84] N. Nagaosa, J. Sinova, S. Onoda, A. H. MacDonald, and N. P. Ong, Anomalous Hall effect, Rev. Mod. Phys. **82**, 1539 (2010).

[85] S. Gholizadeh, J. H. Cullen, and D. Culcer, Nonlinear Hall effect of magnetized two-dimensional spin-$\frac{3}{2}$ heavy holes, Phys. Rev. B **107**, L041301 (2023).

[86] K. Nakazawa, H. F. Legg, J. Klinovaja, and D. Loss, Interband contributions to nonlinear transport in semiconductor nanostructures, Phys. Rev. B **111**, 125305 (2025).

[87] M. Suárez-Rodríguez, B. Martín-García, W. Skowroński, F. Calavalle, S. S. Tsirkin, I. Souza, F. De Juan, A. Chuvilin, A. Fert, M. Gobbi, F. Casanova, and L. E. Hueso, Odd nonlinear conductivity under spatial inversion in chiral tellurium, Phys. Rev. Lett. **132**, 046303 (2024).

[88] Z.-Y. Cao, A.-Q. Wang, X.-Y. Liu, T.-Y. Zhao, D. Yu, and Z.-M. Liao, Nonlinear Hall effect and scaling law analysis in twisted bilayer WSe_2, Phys. Rev. B **111**, 125407 (2025).

[89] Y.-X. Huang, C. Xiao, S. A. Yang, and X. Li, Scaling law and extrinsic mechanisms for time-reversal-odd second-order nonlinear transport, Phys. Rev. B **111**, 155127 (2025).

[90] J.-S. You, S. Fang, S.-Y. Xu, E. Kaxiras, and T. Low, Berry curvature dipole current in the transition metal dichalcogenides family, Phys. Rev. B **98**, 121109(R) (2018).

[91] D.-F. Shao, S.-H. Zhang, G. Gurung, W. Yang, and E. Y. Tsymbal, Nonlinear anomalous Hall effect for Néel vector detection, Phys. Rev. Lett. **124**, 067203 (2020).

[92] C.-H. Park, N. Bonini, T. Sohier, G. Samsonidze, B. Kozinsky, M. Calandra, F. Mauri, and N. Marzari, Electron–phonon interactions and the intrinsic electrical resistivity of graphene, Nano Lett. **14**, 1113 (2014).

[93] T. Sohier, M. Calandra, C.-H. Park, N. Bonini, N. Marzari, and F. Mauri, Phonon-limited resistivity of graphene by first-principles calculations: Electron-phonon interactions, strain-induced gauge field, and Boltzmann equation, Phys. Rev. B **90**, 125414 (2014).